Dark Matter Benchmark Models for Early LHC Run-2 Searches: Report of the ATLAS/CMS Dark Matter Forum

ATLAS+CMS Dark Matter Forum, The authors

Abstract

This document is the final report of the ATLAS-CMS Dark Matter Forum, a forum organized by the ATLAS and CMS collaborations with the participation of experts on theories of Dark Matter, to select a minimal basis set of dark matter simplified models that should support the design of the early LHC Run-2 searches. A prioritized, compact set of benchmark models is proposed, accompanied by studies of the parameter space of these models and a repository of generator implementations. This report also addresses how to apply the Effective Field Theory formalism for collider searches and present the results of such interpretations.

Keywords: `elsarticle.cls`, LaTeX, Elsevier, template

2010 MSC: 00-01, 99-00

Contents

1. Introduction

Dark matter (DM) [1] has not yet been observed in particle physics experiments, and there is not yet any evidence for non-gravitational interactions

[1] Many theories of physics beyond the Standard Model predict the existence of stable, neutral, weakly-interacting and massive particles that are putative DM candidates. In the following, we refer to such matter as DM, even though the observation of such matter at a collider could only establish that it is neutral, weakly-interactive, massive and stable on the distance-scales of tens of meters.

between DM and the Standard Model (SM) particles. If such interactions exist, particles of DM could be produced at the LHC. Since DM particles themselves do not produce signals in the LHC detectors, one way to observe them is when they are produced in association with a visible SM particle X($=g, q, \gamma, Z, W$, or h). Such reactions, which are observed at colliders as particles or jets recoiling against an invisible state, are called "mono-X" or $\not{E}_T$+X reactions (see e.g Refs. [? ? ? ? ?]), where $\not{E}_T$ is the missing transverse momentum observable in the detector.

Early Tevatron and LHC Run-1 searches for $\not{E}_T$+X signatures at CDF [?], ATLAS [? ? ? ? ? ? ? ?] and CMS [? ? ? ? ? ? ?], employed a basis of contact interaction operators in effective field theories (EFTs) [? ?] to calculate the possible signals. These EFTs assume that production of DM takes place through a contact interaction involving a quark-antiquark pair, or two gluons, and two DM particles. In this case, the missing energy distribution of the signal is determined by the nature and the mass of the DM particles and the Lorentz structure of the interaction. Only the overall production rate is a free parameter to be constrained or measured. Provided that the contact interaction approximation holds, these EFTs provide a straightforward way to compare the results from different collider searches with non-collider searches for DM.

The EFT describes the case when the mediator of the interaction between SM and DM particles are very heavy; if this is not the case, models that explicitly include these mediators are needed [? ? ? ? ? ? ? ?]. Some "simplified models" [? ? ?] of DM production were constructed, including particles and interactions beyond the SM. These models can be used consistently at LHC energies, and provide an extension to the EFT approach. Many proposals for such models have emerged (see, for example Refs. [? ? ? ? ? ? ? ? ? ? ? ? ? ? ? ? ? ?]). At the LHC, the kinematics of mono-X reactions occurring via a TeV-scale mediator can differ substantially from the prediction of the contact interaction. The mediator may also produce qualitatively different signals, such as decays back into the SM particles. Thus, appropriate simplified mod-

els are an important component of the design, optimization, and interpretation of DM searches at ATLAS and CMS. This has already been recognized in the CDF, ATLAS and CMS searches quoted above, where both EFT and selected simplified model results are presented.

1.1. The ATLAS/CMS Dark Matter Forum

To understand what signal models should be considered for the upcoming LHC Run-2, groups of experimenters from both ATLAS and CMS collaborations have held separate meetings with small groups of theorists, and discussed further at the DM@LHC workshop [**? ? ?**]. These discussions identified overlapping sets of simplified models as possible benchmarks for early LHC Run-2 searches. Following the DM@LHC workshop, ATLAS and CMS organized a forum, called the *ATLAS-CMS Dark Matter Forum*, to form a consensus on the use of these simplified models and EFTs for early Run-2 searches with the participation of experts on theories of DM. This is the final report of the ATLAS-CMS Dark Matter Forum.

One of the guiding principles of this report is to channel the efforts of the ATLAS and CMS collaborations towards a minimal basis of dark matter models that should influence the design of the early Run-2 searches. At the same time, a thorough survey of realistic collider signals of DM is a crucial input to the overall design of the search program.

The goal of this report is such a survey, though confined within some broad assumptions and focused on benchmarks for kinematically-distinct signals which are most urgently needed. As far as time and resources have allowed, the assumptions have been carefully motivated by theoretical consensus and comparisons of simulations. But, to achieve such a consensus in only a few months before the start of Run-2, it was important to restrict the scope and timescale to the following:

1. The forum should propose a prioritized, compact set of benchmark simplified models that should be agreed upon by both collaborations for Run-2 searches. The values for the scan on the parameters of the models for

which experimental results are provided should be specified, to facilitate theory reinterpretation beyond the necessary model-independent limits that should be provided by all LHC DM searches.

2. The forum should recommend the use of the state of the art calculations for these benchmark models. Such a recommendation will aid the standardization the event generator implementation of the simplified models and the harmonization of other common technical details as far as practical for early Run-2 LHC analyses. It would be desirable to have a common choice of leading order (LO) and next-to-leading order (NLO) matrix elements corresponding to the state of the art calculations, parton shower (PS) matching and merging, factorization and renormalization scales for each of the simplified models. This will also lead to a common set of theory uncertainties, which will facilitate the comparison of results between the two collaborations.
3. The forum should discuss how to apply the EFT formalism and present the results of EFT interpretations.
4. The forum should prepare a report summarizing these items, suitable both as a reference for the internal ATLAS and CMS audiences and as an explanation of early Run-2 LHC benchmark models for theory and non-collider readers. This report represents the views of its endorsers, as participants of the forum.

1.2. Grounding Assumptions

We assume that interactions exist between the SM hadrons and the particles that constitute cosmological DM. If this is not the case, then proton collisions will not directly produce DM particles, and DM will not scatter off nuclei in direct detection experiments.

The DM itself is assumed to be a single particle, a Dirac fermion WIMP, stable on collider timescales and non-interacting with the detector. The former assumption is reductionistic. The rich particle content of the SM is circumstantial evidence that the DM sector, which constitutes five times as much of the

mass of the universe, may be more complex than a single particle or a single interaction. But, as was often the case in the discoveries of the SM, here only one mediator and one search channel might play a dominant role in the opening stages of an LHC discovery. The latter assumption focuses our work on early LHC searches, where small kinematic differences between models will not matter in a discovery scenario, and with the imminent re-start of the LHC our report relies heavily on a large body of existing theoretical work which assumed Dirac fermionic DM.

Different spins of DM particles will typically give similar results. Exceptions exist: For example, the choice of Majorana fermions forbids some processes that are allowed for Dirac fermions [**?**]. Aside from these, adjusting the choice of Dirac or Majorana fermions or scalars will produce only minor changes in the kinematic distributions of the visible particle and is expected to have little effect on cut-and-count[2] analysis. Thus the choice of Dirac fermion DM should be sufficient as benchmarks for the upcoming Run-2 searches.

One advantage of collider experiments lies in their ability to study and possibly characterize the mediator. A discovery of an anomalous $\not{E}_T$ signature at the LHC would not uniquely imply discovery of dark matter, while at the same time e.g. discovery of an anomalous and annually-modulated signal in a direct-detection experiment would leave unanswered many questions about the nature of the interaction that could be resolved by the simultaneous discovery of a new mediator particle. Collider, direct, and indirect detection searches provide complementary ways to approach this problem [**?**], and it is in this spirit that much of our focus is on the mediator.

We systematically explore the basic possibilities for mediators of various possible spins and couplings. All models considered are assumed to produce a signature with pairs of DM particles. Though more varied and interesting

[2]Cut-and-count refers to an analysis that applies a certain event selection and checks the inclusive number of events which pass. This is to be contrasted with a shape analysis, which compares the distribution of events.

possibilities are added to the literature almost daily, these basic building blocks account for much of the physics studied at hadron colliders in the past three decades.

We also assume that Minimal Flavor Violation (MFV) [**? ? ? ?**] applies to the models included in this report. This means that the flavor structure of the couplings between DM and ordinary particles follows the same structure as the SM. This choice is simple, since no additional theory of flavor is required, beyond what is already present in the SM, and it provides a mechanism to ensure that the models do not violate flavor constraints. As a consequence, spin-0 resonances must have couplings to fermions proportional to the SM Higgs couplings. Flavor-safe models can still be constructed beyond the MFV assumption, for example [**?**], and deserve further study. For a discussion of MFV in the context of the simplified models included in this report, see Ref. [**?**].

In the parameter scan for the models considered in this report, we make the assumption of a minimal decay width for the particles mediating the interaction between SM and DM. This means that only decays strictly necessary for the self-consistency of the model (e.g. to DM and to quarks) are accounted for in the definition of the mediator width. We forbid any further decays to other invisible particles of the Dark Sector that may increase the width or produce striking, visible signatures. Studies within this report show that, for cut-and-count analyses, the kinematic distributions of many models, and therefore the sensitivity of these searches, do not depend significantly on the mediator width, as long as the width remains smaller than the mass of the particle and that narrow mediators are sufficiently light.

The particle content of the models chosen as benchmarks is limited to one single kind of DM whose self-interactions are not relevant for LHC phenomenology, and to one type of SM/DM interaction at a time. These assumptions only add a limited number of new particles and new interactions to the SM. These simplified models, independently explored by different experimental analyses, can be used as starting points to build more complete theories. Even though this factorized picture does not always lead to full theories and leaves out details

that are necessary for the self-consistency of single models (e.g. the mass generation for mediator particles), it is a starting point to prepare a set of distinct but complementary collider searches for DM, as it leads to benchmarks that are easily comparable across channels.

1.3. Choices of benchmarks considered in this report and parameter scans

Contact interaction operators have been outlined as basis set of theoretical building blocks representing possible types of interactions between SM and DM particles in [**?**]. The approach followed by LHC searches (see e.g. Refs. [**? ?**] for recent jet+$\not{E}_T$ Run-1 searches with the 8 TeV dataset) so far has been to simulate only a prioritized set of the possible operators with distinct kinematics for the interpretation of the constraints obtained, and provide results that may be reinterpreted in terms of the other operators. This report intends to follow this strategy, firstly focusing on simplified models that allow the exploration of scenarios where the mediating scale is not as large. In the limit of large mediator mass, the simplified models map onto the EFT operators. Secondly, this report considers specific EFT benchmarks whenever neither a simplified model completion nor other simplified models yielding similar kinematic distributions are available and implemented in one of the event generators used by both collaborations. This is the case for dimension-5 or dimension-7 operators with direct DM-electroweak boson couplings [3]. Considering these models as separate experimental benchmarks will allow to target new signal regions and help validate the contact interaction limit of new simplified models developed to complete these specific operators. Results from these EFT benchmarks should include the condition that the momentum transfer does not probe the scale of the interaction; whenever there is no model that allows a direct mapping between these two quantities, various options should be tested to ensure a given

[3] An example of a dimension-5 operator for scalar DM is described in Appendix **??**. Dimension-7 operators of DM coupling to gauge bosons exist in the literature, but they require a larger particle spectrum with respect to the models studied in this report.

fraction of events within the range of applicability of the EFT approach. Experimental searches should in any case deliver results that are independent from the specific benchmark tested, such as fiducial cross-sections that are excluded in a given signal region.

When choosing the points to be scanned in the parameter space of the models, this report does not quantitatively consider constraints that are external to the MET+X analyses. This is the case also for results from LHC experiments searching for mediator decays. The main reason for not doing so in this report is the difficulty of incorporating these constraints in a rigorous quantitative way within the timescale of the Forum. However, even if the parameter scans and the searches are not optimized with those constraints in mind, we intend to make all information available to the community to exploit the unique sensitivity of colliders to all possible DM signatures.

1.4. Structure of this report and dissemination of results

The report provides a brief theoretical summary of the models considered, starting from the set of simplified models and contact interactions put forward in previous discussions and in the literature cited above. Its main body documents the studies done within this Forum to identify a kinematically distinct set of model parameters to be simulated and used as benchmarks for early Run-2 searches. The implementation of these studies according to the state of the art calculations is detailed, including instructions on how to estimate theoretical uncertainties in the generators used for these studies. The presentation of results for EFT benchmarks is also covered.

Chapter 2 of this report is dedicated to simplified models with radiation of a hard object either from the initial state or from the mediator. These models produce primarily monojet signatures, but should be considered for all $\not{E}_T$+X searches. Chapter **??** contains studies on the benchmark models for final states specifically containing an electroweak boson ($W/Z/\gamma/H$). In this case, both simplified models leading to mono-boson signatures and contact interaction operators are considered. Details of the state of the art calculations and on the

implementation of the simplified models in Monte Carlo generators are provided in Chapter **??**. Chapter **??** is devoted to the treatment of the presentation of results for the benchmark models from contact interaction operators. Chapter **??** prescribes how to estimate theoretical uncertainties on the simulation of these models. Chapter **??** concludes the report.

Further models that could be studied beyond early searches and their implementation are described in Appendix **??**. For these models, either the implementation could not be fully developed by the time of this report, or some of the grounding assumptions were not fully met. Some of these models have been used in previous ATLAS and CMS analyses and discussed thoroughly within the Forum. They are therefore worth considering for further studies and for Run-2 searches, since they lead to unique $\not{E}_T$+X signatures that are not shared by any other of the models included in this report. Appendix **??** contains the necessary elements that should be included in the results of experimental searches to allow for further reinterpretation.

It is crucial for the success of the work of this Forum that these studies can be employed as cross-check and reference to the theoretical and experimental community interested in early Run-2 searches. For this reason, model files, parameter cards, and cross-sections for the models considered in these studies are publicly available. The SVN repository of the Forum [**?**] contains the models and parameter files necessary to reproduce the studies within this report. Details and cross-sections for these models, as a function of their parameters, will be published on HEPData [**?**].

2. Simplified models for all $\not{E}_T$ +X analyses

In this Chapter we review models that yield X+$\not{E}_T$ signatures, where X is a QCD parton or γ, W, Z or h.

The primary simplified models for Dirac fermion DM studied and recommended by this Forum for early LHC Run-2 searches are detailed in this Chapter, comprising spin-0 and spin-1 mediators. Section 2.1 covers the s-channel

exchange of a vector mediator [4], while we consider both s-channel and t-channel exchange for scalar mediators in Section 2.2 and 2.3 respectively. Spin-2 mediators are briefly mentioned in Section 3. While these models are general and cover a broad set of signatures, the discussion and studies are focused on the monojet final state. Details on final states with electroweak (EW) boson radiation and with heavy flavor quarks from diagrams arising within these models are also discussed in this Chapter.

A summary of the state of the art calculations and implementations for these models is provided in Table 6.1. Section **??** details the implementation of these models that have been used for the studies in this Chapter and that will be employed for the simulation of early Run-2 benchmark models for LHC DM searches.

2.1. Vector and axial vector mediator, s-channel exchange

A simple extension of the SM is an additional $U(1)$ gauge symmetry, where a DM candidate particle has charges only under this new group. Assuming that some SM particles are also charged under this group, a new gauge boson can mediate interactions between the SM and DM.

We consider the case of a DM particle χ of mass m_χ that is a Dirac fermion and where the production proceeds via the exchange of a spin-1 mediator of mass M_{med} in the s-channel, illustrated in Fig. 1.

We consider two models with vector and axial-vector couplings between the spin-1 mediator Z' and SM and DM fields, with the corresponding interaction Lagrangians:

[4] Colored vector mediators can be exchanged in the t-channel, but there are no examples in literature so far.

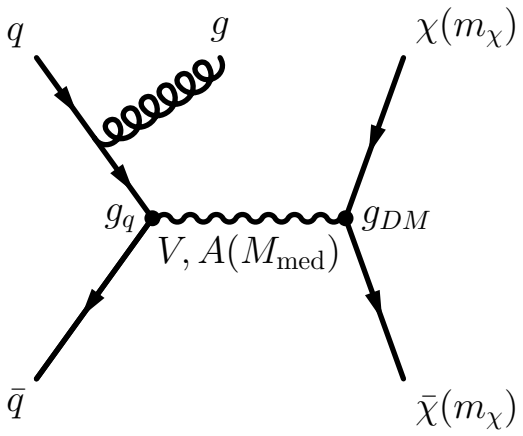

Figure 1: Representative Feynman diagram showing the pair production of DM particles in association with a parton from the initial state via a vector or axial-vector mediator. The cross section and kinematics depend upon the mediator and DM masses, and the mediator couplings to DM and quarks respectively: ($M_{\rm med}$, m_χ, g_χ, $g_{\rm q}$).

$$\mathcal{L}_{\rm vector} = g_{\rm q} \sum_{q=u,d,s,c,b,t} Z'_\mu \bar{q}\gamma^\mu q + g_\chi Z'_\mu \bar{\chi}\gamma^\mu \chi \tag{1}$$

$$\mathcal{L}_{\rm axial-vector} = g_{\rm q} \sum_{q=u,d,s,c,b,t} Z'_\mu \bar{q}\gamma^\mu\gamma^5 q + g_\chi Z'_\mu \bar{\chi}\gamma^\mu\gamma^5 \chi. \tag{2}$$

The coupling $g_{\rm q}$ is assumed to be universal to all quarks. It is also possible to consider other models in which mixed vector and axial-vector couplings are considered, for instance the couplings to the quarks are axial-vector whereas those to DM are vector.

As mentioned in the Introduction, when no additional visible or invisible decays contribute to the width of the mediator, the minimal width is fixed by the choices of couplings $g_{\rm q}$ and g_χ. The effect of larger widths is discussed in Section 4.2. For the vector and axial-vector models, the minimal width is:

$$\Gamma^{\mathrm{V}}_{\mathrm{min}} = \frac{g_\chi^2 M_{\mathrm{med}}}{12\pi}\left(1+\frac{2m_\chi^2}{M_{\mathrm{med}}^2}\right)\beta_{DM}\theta(M_{\mathrm{med}}-2m_\chi) \tag{3}$$
$$+\sum_q \frac{3g_{\mathrm{q}}^2 M_{\mathrm{med}}}{12\pi}\left(1+\frac{2m_q^2}{M_{\mathrm{med}}^2}\right)\beta_q\theta(M_{\mathrm{med}}-2m_q),$$
$$\Gamma^{\mathrm{A}}_{\mathrm{min}} = \frac{g_\chi^2 M_{\mathrm{med}}}{12\pi}\beta_{DM}^3\theta(M_{\mathrm{med}}-2m_\chi) \tag{4}$$
$$+\sum_q \frac{3g_{\mathrm{q}}^2 M_{\mathrm{med}}}{12\pi}\beta_q^3\theta(M_{\mathrm{med}}-2m_q)\ .$$

$\theta(x)$ denotes the Heaviside step function, and $\beta_f = \sqrt{1-\frac{4m_f^2}{M_{\mathrm{med}}^2}}$ is the velocity of the fermion f with mass m_f in the mediator rest frame. Note the color factor 3 in the quark terms. Figure 2 shows the minimal width as a function of mediator mass for both vector and axial-vector mediators assuming the coupling choice $g_{\mathrm{q}} = g_\chi = 1$. With this choice of the couplings, the dominant contribution to the minimal width comes from the quarks, due to the combined quark number and color factor enhancement. We specifically assume that the vector mediator does not couple to leptons. If such a coupling were present, it would have a minor effect in increasing the mediator width, but it would also bring in constraints from measurements of the Drell-Yan process that would unnecessarily restrict the model space.

Therefore, the minimal set of parameters under consideration for these two models is

$$\{\ g_{\mathrm{q}},\ g_\chi,\ m_\chi,\ M_{\mathrm{med}},\}\ . \tag{5}$$

together with the spin structure of their couplings.

A thorough discussion of these models and their parameters can also be found in [**?**].

These simplified models are known and available in event generators at NLO + PS accuracy, as detailed in Section **??**. Results in this Section have been obtained using the model implementation within the POWHEG generator (v3359) [**?**], interfaced to Pythia 8 [**?**] for the parton shower.

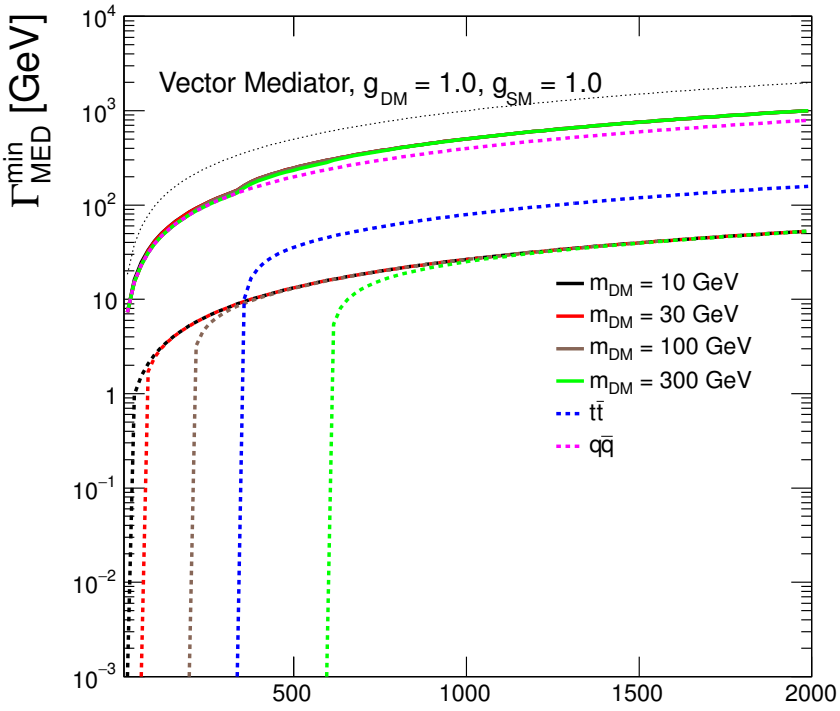

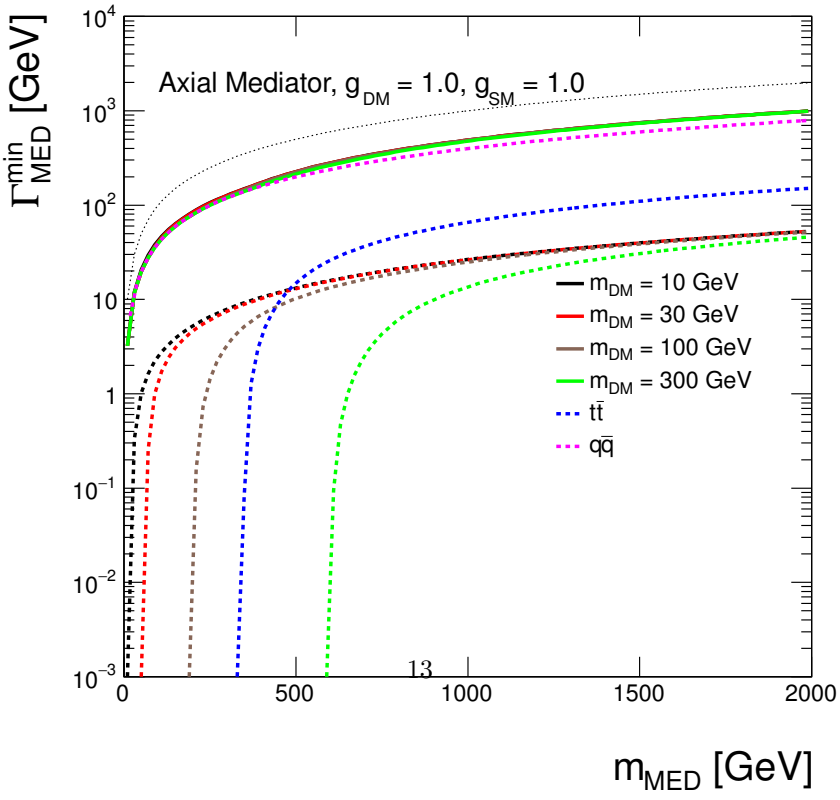

Figure 2: Minimal width as a function of mediator mass for vector and axial-vector mediator assuming couplings of 1. The total width is shown as solid lines for DM masses of 10 GeV,

In addition, for the vector models considered, initial and final state radiation of a Z' can occur which can appear as a narrow jet if it decays hadronically and may not be distinguishable from a QCD jet, thus accounting for some fraction of the monojet signal. The ISR and FSR of Z' becomes more important at large values of the couplings [**?**].

2.1.1. Parameter scan

In order to determine an optimal choice of the parameter grid for the simulation of early Run-2 benchmark models, dependencies of the kinematic quantities and cross sections on the model parameters have been studied. Only points that are kinematically distinct will be fully simulated, while instructions on how to rescale the results according to models with different cross sections are presented in Section 4. The following paragraphs list the main observations from the scans over the parameters that support the final proposal for the benchmark signal grid.

Scan over the couplings. To study the dependence of kinematic distributions on the coupling strength, samples were generated where a pair of $m_\chi = 10$ GeV DM particles is produced on-shell from the mediator of $M_{\text{med}} = 1$ TeV. Figure 3 compares the shapes of the $\not{E}_T$ distribution for the different choices of the coupling strength. This is a generator-level prediction with no kinematic selections or detector simulation. Coupling values in the scan range 0.1–1.45, fixing $g_{\text{q}} = g_\chi$, correspond to a rough estimate of the lower sensitivity of mono-jet analyses and a maximum coupling value such that $\Gamma_{\text{min}} < M_{\text{med}}$. We observe that the shapes of the $\not{E}_T$ or jet p_{T} distributions do not depend on the couplings (and consequently the width) in the ranges considered. A large width of the mediator implies a broad integral over the contributing parton distributions, which might not be well approximated by the midpoint of this integral. This study shows that the effect, in the p_{T} distribution of the observed gluon, is not important.

Based on similar findings for different choices of M_{med} and m_χ, we conclude that the shapes of kinematic distributions are not altered by coupling variations,

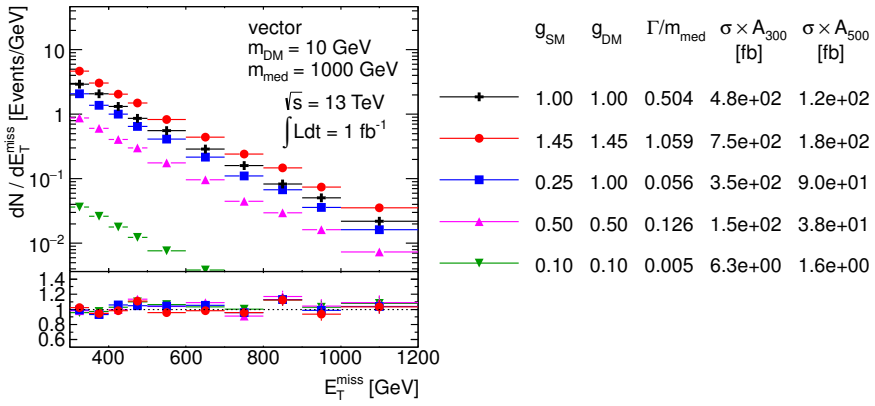

Figure 3: Scan over couplings. The $\not{E}_T$ distribution is compared for the vector mediator models using the parameters as indicated. Ratios of the normalized distributions with respect to the first one are shown. A_{300} and A_{500} in the table denote the acceptance of the $\not{E}_T > 300$ GeV and $\not{E}_T > 500$ GeV cut, respectively. All figures in this Section have been obtained using the model implementation within the POWHEG generator (v3359) [**?**], interfaced to Pythia 8 [**?**] for the parton shower.

neither for the on-shell mediator case where $M_{\rm med} > 2m_\chi$, nor for the off-shell case where $M_{\rm med} < 2m_\chi$. Only the production cross sections change. Differences in kinematic distributions are expected only close to the transition region between on-shell and off-shell mediators.

Special care needs to be taken when coupling strengths are combined with extremely heavy mediators. Figure 4 suggests a change in the shape of the $\not{E}_T$ distribution for a $M_{\rm med} = 5$ TeV mediator once $\Gamma_{\rm min}/M_{\rm med}$ is of the order of a percent or lower.

Such heavy mediators, although inaccessible with early LHC data, are interesting since they provide a good approximation for benchmark EFT models. The observed difference among the simplified models in the plot arises from the fact that the region of low invariant masses of the DM pair, $m_{\bar{\chi}\chi}$, is suppressed due to narrow Breit-Wigner peak that only probes a narrow window of parton distribution functions. For wider mediators, the low mass region is significantly enhanced by parton distribution functions at low Bjorken x, as illustrated in

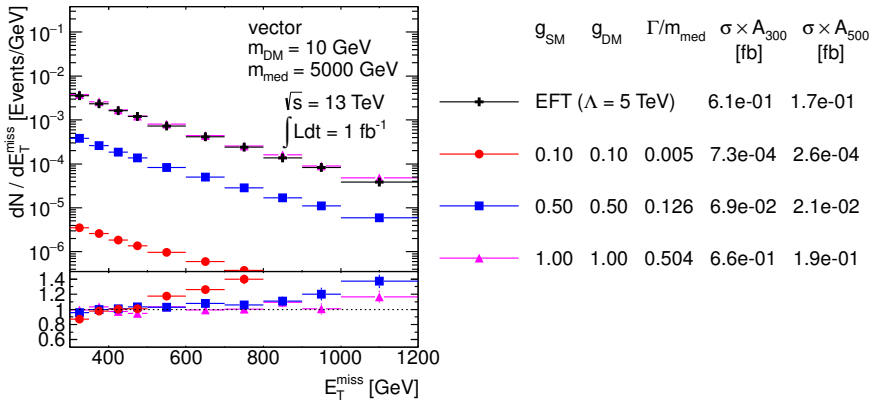

Figure 4: Comparison of the $\not{E}_T$ distributions from the D5 EFT sample and the vector models with 5 TeV heavy mediator of various widths. Ratios of the normalized distributions with respect to the first one are shown. A_{300} and A_{500} in the table denote the acceptance of the $\not{E}_T > 300$ GeV and $\not{E}_T > 500$ GeV cut, respectively.

Fig. 5(a). This explains why the sample with the narrowest mediator in Fig. 4 is heavily suppressed in terms of production cross section and also gives different $\not{E}_T$ shape. Furthermore, Fig. 4 compares the vector model with 5 TeV mediator to the D5 EFT sample and reveals that the simplified models with larger mediator widths (e.g. for couplings of 1 where $\Gamma_{\rm min}/M_{\rm med} \sim 0.5$) are the ones resembling the kinematics of contact interactions. This reflects the fact that in an EFT there is no enhancement due to on-shell mediators, leading to a closer resemblance to an off-shell regime where no peak in the $m_{\bar{\chi}\chi}$ distribution is present. In case of narrow width mediators, e.g. $\Gamma_{\rm min}/M_{\rm med} \sim 0.05$, even larger mediator masses need to be chosen in order to significantly suppress the peak in the $m_{\bar{\chi}\chi}$ distribution and reproduce the kinematic shapes of an EFT model. Figure 5(b) verifies that the choice of 10 TeV mediator mass is sufficient to achieve that.

Since kinematic distributions are robust to changes in the specific values of coupling [5], the choice of $g_{\rm q}$ =0.25 and g_χ =1 is reasonable to reduce the

[5] This applies as long as heavy narrow mediators are generated without any truncation of

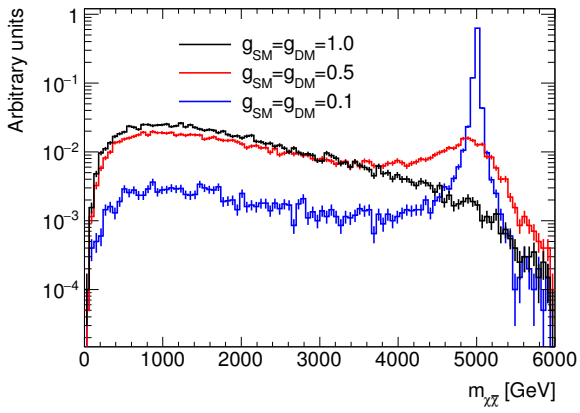

(a)

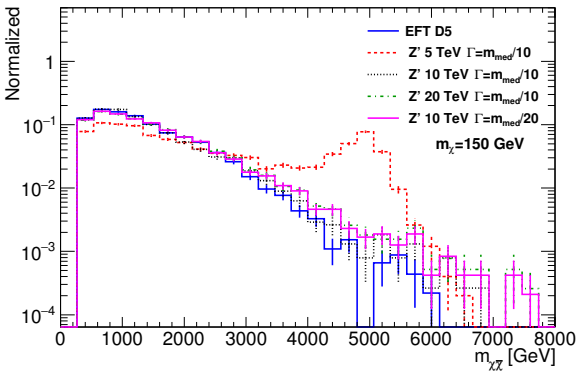

(b)

Figure 5: Invariant mass of the DM pair in the vector mediator samples with $m_\chi = 10$ GeV, $M_{\text{med}} = 5$ TeV and different coupling strengths (a). A similar comparison is shown for the samples with different mediator masses considering $\Gamma_{\text{min}}/M_{\text{med}} = 0.05$ and 0.1 (b). An EFT sample is also displayed in the latter case. The distributions are normalised to unit area.

parameter space to be scanned. There are no complications associated with small couplings, but, also, the early part of Run 2 will not be sensitive to them. The range of couplings we recommend to generate limit the calculated width of the mediator to be near or below $M_{\rm med}$.

For direct mediator searches, such as $q\bar{q} \to Z' \to q\bar{q}$, different couplings ($g_{\rm q} \neq g_\chi$) might also be considered. A scan in g_χ vs $g_{\rm q}$ can then be performed for a fixed mediator mass. Such searches may restrict $g_{\rm q}$ to a greater degree than g_χ.

Scan over m_χ. For a fixed mediator mass $M_{\rm med}$ and couplings, the DM mass falls into three regimes:

On-shell: When $M_{\rm med} \gg 2m_\chi$, most mediators are on-shell. The hardness of the ISR is set by $M_{\rm med}$, and the kinematic distributions do not strongly depend on m_χ. This is illustrated in Fig. 6 for an example of $M_{\rm med}$ =1 TeV 10 GeV $< m_\chi <$ 300 GeV. The cross section decreases as the m_χ approaches $M_{\rm med}/2$. A coarse binning along m_χ is sufficient.

Threshold: When $M_{\rm med} \approx 2m_\chi$, the production is resonantly enhanced, and both the cross section and kinematic distributions change more rapidly as a function of the two masses, and finer binning is needed in order to capture the changes.

Off-shell: When $M_{\rm med} \ll 2m_\chi$, the DM pair is produced by an off-shell mediator. The mediator propagator gives an explicit suppression of $(M_{\rm med}/Q)^2$ that suppresses hard ISR. The $m_\chi = 1$ TeV case, shown in Fig. 6, and Figure 7 demonstrates that the $\not\!\!E_T$ spectrum hardens with increasing m_χ, accompanied by the gradual decrease of the cross section. Due to the significant cross section suppression, it is not necessary to fully populate the parameter space. Imminent LHC searches are not expected to be sensitive to these signals.

low-mass tails at the generator-level.

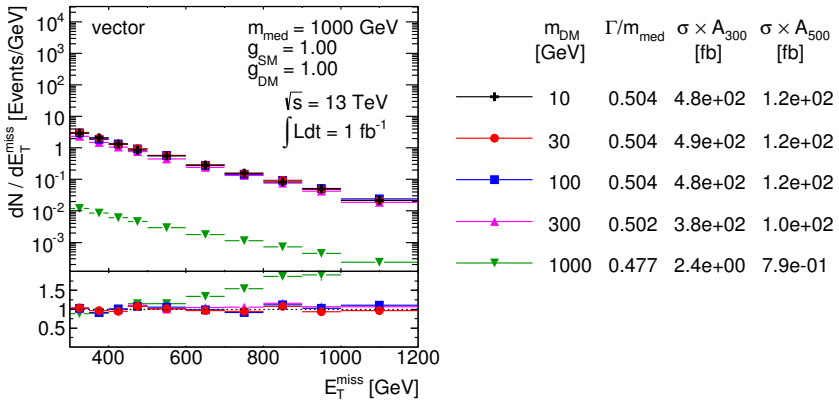

Figure 6: Scan over DM mass. The $\not{E}_T$ distribution is compared for the vector mediator models using the parameters as indicated. Ratios of the normalized distributions with respect to the first one are shown. A_{300} and A_{500} in the table denote the acceptance of the $\not{E}_T >$ 300 GeV and $\not{E}_T > 500$ GeV cut, respectively.

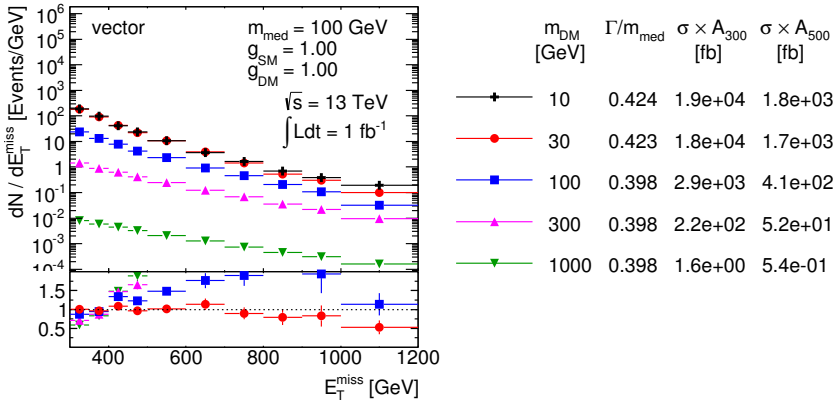

Figure 7: Scan over DM mass. The $\not{E}_T$ distribution is compared for the vector mediator models using the parameters as indicated. Ratios of the normalized distributions with respect to the first one are shown. A_{300} and A_{500} in the table denote the acceptance of the $\not{E}_T >$ 300 GeV and $\not{E}_T > 500$ GeV cut, respectively.

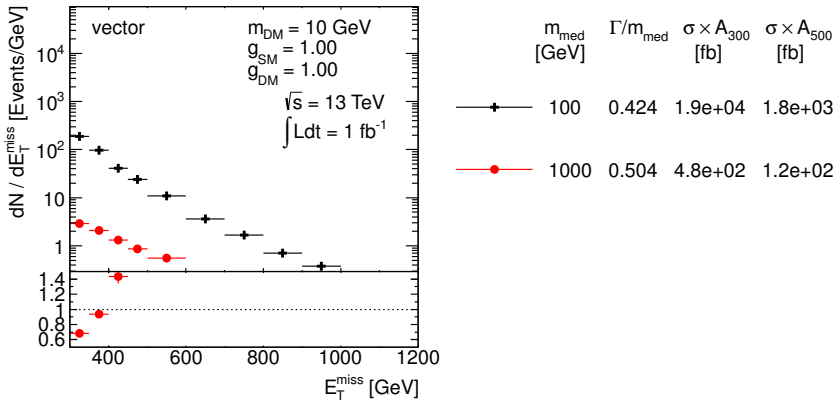

Figure 8: Scan over mediator mass. The $\not{E}_T$ distribution is compared for the vector mediator models using the parameters as indicated. Ratios of the normalized distributions with respect to the first one are shown. A_{300} and A_{500} in the table denote the acceptance of the $\not{E}_T > 300$ GeV and $\not{E}_T > 500$ GeV cut, respectively.

Scan over the mediator mass. Changing the mediator mass for fixed DM mass and couplings leads to significant differences in cross section and shapes of the kinematic variables for the on-shell regime, as shown in Fig. 8. As expected, higher mediator masses lead to harder $\not{E}_T$ spectra. On the other hand, the $\not{E}_T$ shapes are similar for off-shell mediators. This is illustrated in Fig. 9. Therefore, a coarse binning in M_{med} is sufficient in the off-shell regime.

Spin structure of the couplings. This section compares the kinematic properties of vector, axial-vector and mixed vector/axial-vector models. The samples with pure vector and pure axial-vector couplings are compared for $M_{\text{med}} = 100$ GeV and different DM masses in Fig. 10. No differences in the shape of the $\not{E}_T$ distributions are observed between the samples with coincident masses. In the case of the on-shell mediators, where $2m_\chi \ll M_{\text{med}}$, the cross sections of the pure vector and pure axial-vector models are similar. With increasing DM mass towards the $2m_\chi = M_{\text{med}}$ transition and further into the off-shell regime, the relative difference between the cross sections of the two samples is increasing, with the vector ones having larger cross sections.

Figure 11 shows the samples generated with pure and mixed couplings for

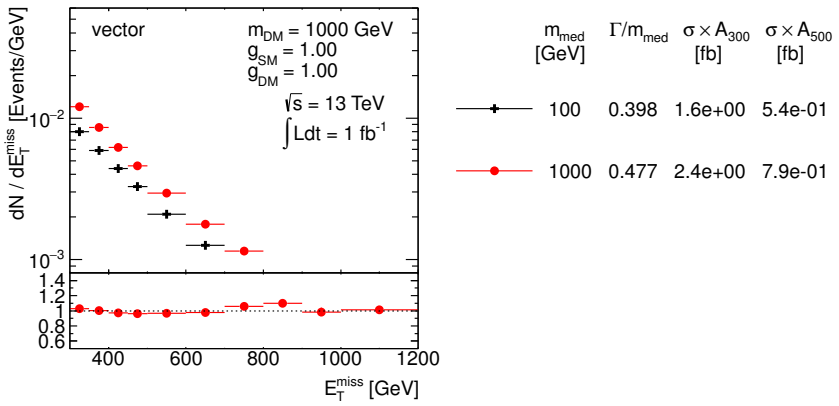

Figure 9: Scan over mediator mass. The $\not{E}_T$ distribution is compared for the vector mediator models using the parameters as indicated. Ratios of the normalized distributions with respect to the first one are shown. A_{300} and A_{500} in the table denote the acceptance of the $\not{E}_T > 300$ GeV and $\not{E}_T > 500$ GeV cut, respectively.

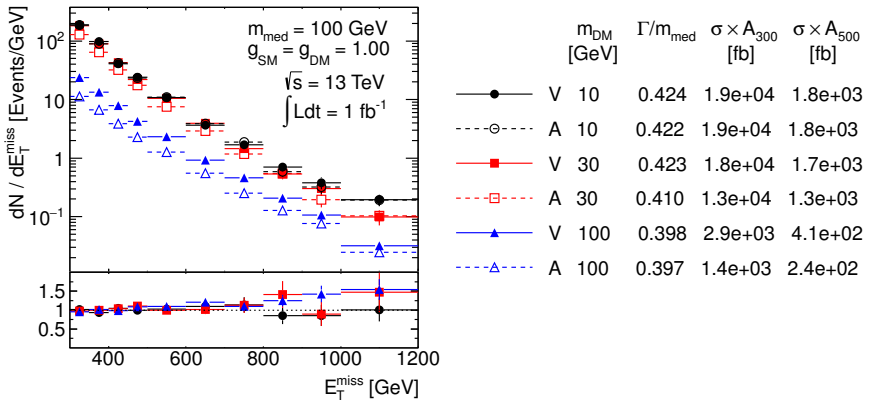

Figure 10: Comparison of the pure vector and pure axial-vector couplings. The $\not{E}_T$ distribution is shown for the samples generated with $M_{\text{med}} = 100$ GeV and different DM masses. Ratios of the normalized distributions are shown for between the samples with coincident masses. A_{300} and A_{500} in the table denote the acceptance of the $\not{E}_T > 300$ GeV and $\not{E}_T > 500$ GeV cut, respectively.

$m_\chi = 100$ GeV and $M_{\text{med}} = 1$ TeV, i.e. where the mediator is on-shell. The mediator width between the pure vector and pure axial-vector couplings differ only by 2% in this case, and $< 10\%$ agreement between the cross sections is found. The mediator widths for the samples with the same type coupling to quarks agree at better than 1% since the width is dominated by the quark contribution, as expected from Eq. 3. No significant differences between the samples with same type DM coupling are seen, given the statistical precision of the generated samples. This is expected since the mediator is on-shell, and the details of the invisible decay are unimportant in cut-and-count searches.

For the off-shell case, shown in Fig. 12 for $m_\chi = 100$ GeV and $M_{\text{med}} = 100$ GeV, there is approximately a factor 2 difference between the cross-sections of the samples with pure couplings is observed. As in the previous case, the samples with the same type coupling to DM are similar both in terms of cross sections and $\not{E}_T$ shape. Since the contribution to the mediator width from DM is closed in this case, only the quark couplings define the width. Only couplings to light quarks are opened in the case of $M_{\text{med}} = 100$ GeV for which the differences between the partial widths of vector and axial-vector couplings are marginal. This explains the similar minimal widths for all four samples stated in Fig. 12.

In general, the coupling to quarks is not expected to play an important role in the kinematics as it is only needed to produce the mediator which is confirmed by the observations above. Based on this argument and on the observations above, we recommend to consider only the models with pure vector couplings or pure axial-vector couplings for simulation.

Proposed parameter grid. The final step in proposing a parameter grid is to evaluate the sensitivity of Run-2 LHC data with respect to rate and/or kinematics. The parameter scan focuses on two important regions, the light mediator region and the heavy mediator limit to reproduce the EFT limit, and takes into account the projected sensitivities for the mono-jet analysis.

Considering simplified models also allows to discuss constraints from different search channels. In the case of the s-channel exchange, the results from the

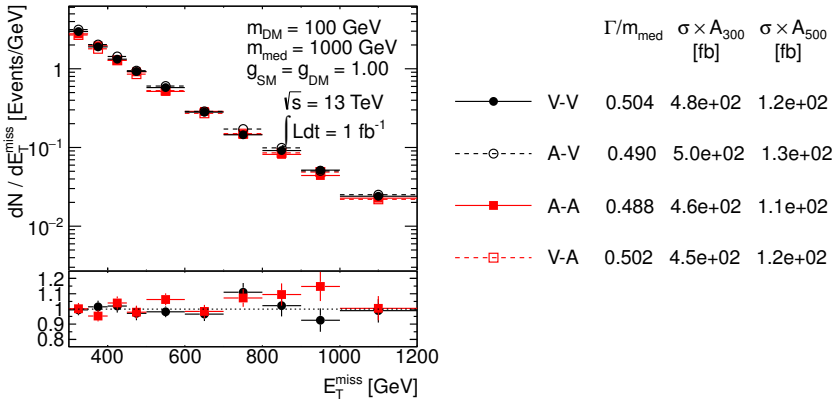

Figure 11: Comparison of the pure vector, V-V, and pure axial-vector, A-A, couplings with mixed couplings, A-V and V-A where the first (second) letter indicates the SM (dark sector) vertex. The $\not{E}_T$ distribution is shown for the samples generated with $m_\chi = 100$ GeV and $M_{\text{med}} = 1$ TeV. Ratios of the normalized distributions are shown for A-V over V-V and for V-A over A-A. A_{300} and A_{500} in the table denote the acceptance of the $\not{E}_T > 300$ GeV and $\not{E}_T > 500$ GeV cut, respectively.

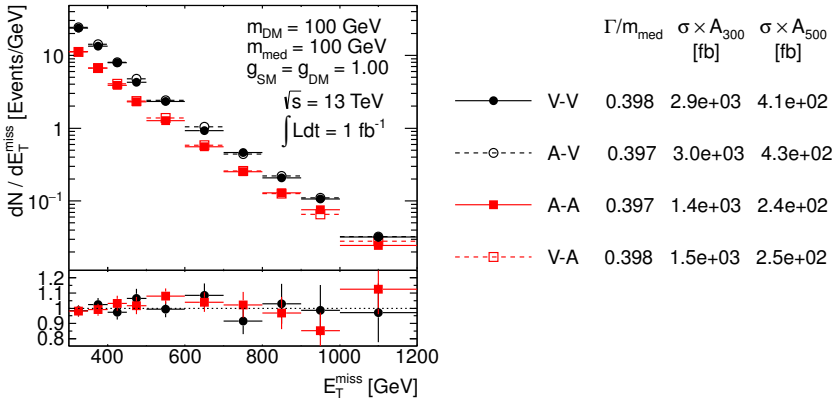

Figure 12: Comparison of the pure vector, V-V, and pure axial-vector, A-A, couplings with mixed couplings, A-V and V-A where the first (second) letter indicates the SM (dark sector) vertex. The $\not{E}_T$ distribution is shown for the samples generated with $m_\chi = 100$ GeV and $M_{\text{med}} = 100$ GeV. Ratios of the normalized distributions are shown for A-V over V-V and for V-A over A-A. A_{300} and A_{500} in the table denote the acceptance of the $\not{E}_T > 300$ GeV and $\not{E}_T > 500$ GeV cut, respectively. The suppression by β^3 for $m_\chi \sim M_{\text{med}}$ can be seen for the curves representing axial DM coupling.

mono-jet final states, where the mediator decays to a DM pair, one can also take into account dijet constraints on the processes where the mediator decays back to the SM particles. The importance of the dijet results depend on the magnitude of the coupling g_{q}. We recommend to keep the two channels rather independent by choosing $g_{\mathrm{q}} = 0.25$ and $g_{\chi} = 1$, based on the findings given in Ref. [**?**]. Furthermore, it is also important to mention this choice leads to $\Gamma_{\mathrm{min}}/M_{\mathrm{med}} \lesssim 0.06$. Note that the usual choice of $g_{\mathrm{q}} = g_{\chi} = 1$ used in literature leads to $\Gamma_{\mathrm{min}}/M_{\mathrm{med}} \sim 0.5$, questioning the applicability of the narrow width approximation.

The expected upper limit at 95% confidence level on the product of cross section, acceptance and efficiency, $\sigma \times A \times \epsilon$, in the final Run-1 ATLAS mono-jet analysis [**?**] is 51 fb and 7.2 fb for $\not{E}_T > 300$ GeV and $\not{E}_T > 500$ GeV, respectively. Projected sensitivities for a 14 TeV mono-jet analysis are available from ATLAS [**?**]. These ATLAS studies estimate a factor of two increase in sensitivity with the 2015 data. The generator level cross section times efficiency times acceptance at $\not{E}_T > 500$ GeV for the model with couplings $g_{\mathrm{q}} = 0.25$ and $g_{\chi} = 1$, a light DM particle of m_{χ} =10 GeV and a M_{med} =1 TeV vector mediator is at the order of 100 fb, i.e. the early Run-2 mono-jet analysis is going to be sensitive to heavier mediators than this. The value of $\sigma \times \epsilon \times A$ at $\not{E}_T > 500$ GeV for a 5 TeV vector mediator is at the order of 0.1 fb, therefore this model lies beyond the reach of the LHC in the early Run-2. However, models with high enough mediators are still useful to reproduce the EFT result.

Following these arguments, M_{med} grid points are chosen, roughly equidistant in a logarithmic scale: 10 GeV, 20 GeV, 50 GeV, 100 GeV, 200 GeV, 300 GeV, 500 GeV, 1000 GeV and 2000 GeV. In the threshold regime $M_{\mathrm{med}} = 2m_{\chi}$, the m_{χ} grid points are taken at approximately $M_{\mathrm{med}}/2$, namely: 10 GeV, 50 GeV, 150 GeV, 500 GeV and 1000 GeV. Points on the on-shell diagonal are always chosen to be 5 GeV away from the threshold, to avoid numerical instabilities in the event generation. The detailed studies of the impact of the parameter changes on the cross section and kinematic distributions presented earlier in this section support removing some of the grid points and relying on interpolation.

The optimized grids proposed for the vector and axial-vector mediators are given in Table. 1. One point at very high mediator mass (10 TeV) is added for each of the DM masses scanned, to aid the reinterpretation of results in terms of contact interaction operators (EFTs), as discussed in Section **??**.

m_χ/ GeV	$M_{\rm med}$/ GeV									
1	10	20	50	100	200	300	500	1000	2000	10000
10	10	15	50	100						10000
50	10		50	95	200	300				10000
150	10				200	295	500	1000		10000
500	10						500	995	2000	10000
1000	10							1000	1995	10000

Table 1: Simplified model benchmarks for s-channel simplified models (spin-1 mediators decaying to Dirac DM fermions in the V and A case, taking the minimum width for $g_{\rm q} = 0.25$ and $g_\chi = 1$)

.

Tables 2 and 3 give the $\Gamma_{\rm min}/M_{\rm med}$ ratio for the parameter grid proposed for vector and axial-vector s-channel models, respectively. The numbers range from ~ 0.02 in the off-shell regime at $2m_\chi > M_{\rm med}$ to ~ 0.06 in the on-shell regime for heavy mediators where all coupling channels contribute.

2.1.2. Additional considerations for V+$\not{E}_T$ signatures

All models detailed in this Section are applicable to signatures where a photon, a W boson, a Z boson or a Higgs boson is radiated from the initial state partons instead of a gluon. The experimental signature is identified as V+$\not{E}_T$ and it has been sought by ATLAS and CMS in Refs. [**? ? ? ? ? ?**]. This signature is also produced by the models described in Section **??**.

Monojet searches are generally more sensitive with respect to final states including EW bosons, due to the much larger rates of signal events featuring quark or gluon radiation with respect to radiation of bosons [**?**], in combination with the low branching ratios if leptons from boson decays are required in the

m_χ/ GeV	M_{med}/ GeV									
	10	20	50	100	200	300	500	1000	2000	10000
1	0.049	0.051	0.051	0.051	0.051	0.051	0.056	0.056	0.056	0.056
10	0.022	0.024	0.054	0.052						0.056
50	0.022		0.025	0.025	0.055	0.053				0.056
150	0.022				0.025	0.025	0.061	0.058		0.056
500	0.022						0.029	0.030	0.060	0.057
1000	0.022							0.030	0.030	0.057

Table 2: Minimal width of the vector mediator exchanged in s-channel divided by its mass, assuming $g_{\text{q}} = 0.25$ and $g_\chi = 1$. The numbers tabulated under $2m_\chi = M_{\text{med}}$ correspond to the width calculated for $M_{\text{med}} - 5$ GeV.

m_χ/ GeV	M_{med}/ GeV									
	10	20	50	100	200	300	500	1000	2000	10000
1	0.045	0.049	0.051	0.051	0.051	0.051	0.053	0.055	0.056	0.056
10	0.020	0.022	0.047	0.050						0.056
50	0.020		0.025	0.025	0.045	0.048				0.056
150	0.020				0.025	0.025	0.044	0.053		0.056
500	0.020						0.027	0.029	0.050	0.056
1000	0.020							0.029	0.030	0.055

Table 3: Minimal width of the axial-vector mediator exchanged in s-channel divided by its mass, assuming $g_{\text{q}} = 0.25$ and $g_\chi = 1$. The numbers tabulated under $2m_\chi = M_{\text{med}}$ correspond to the width calculated for $M_{\text{med}} - 5$ GeV.

final state. The rates for the Higgs boson radiation is too low for these models to be considered a viable benchmark [**?**]. However, the presence of photons, leptons from W and Z decays, and W or Z bosons decaying hadronically allow backgrounds to be rejected more effectively, making $Z/\gamma/W+\not{E}_T$ searches still worth comparing with searches in the jet+$\not{E}_T$ final state (see e.g. Ref. [**?**]).

In the case of a spin-1 mediator, an example Feynman diagram for these processes can be constructed by taking Fig. 1 and replacing the gluon with γ, W or Z.

When the initial state radiation is a W boson, Run-1 searches have considered three benchmark cases, varying the relative coupling of the W to u and d quarks. The simplified model with a vector mediator mediator exchanged in the s-channel includes only the simplest of these cases, in which the W coupling to u and d quarks is identical, as required naively by SU(2) gauge invariance. With some more complex model building, other cases are possible. The case in which the u and d couplings have opposite sign is particularly interesting, since this enhances the $W + \not{E}_T$ signal over the jet+$\not{E}_T$ signal [**? ? ?**]. An example of a model of this type is discussed in Appendix **??**.

Simulations for the models in this Section have been done at the LO+PS level using MadGraph5_aMC@NLO 2.2.3 interfaced to Pythia 8, and therefore no special runtime configuration is needed for pythia 8. Even though merging samples with different parton multiplicities is possible, this has not been deemed necessary as the visible signal comes from the production of a heavy SM boson whose transverse momentum distribution is sufficiently well described at LO+PS level.

In these $V+\not{E}_T$ models, as in the case of the jet+$\not{E}_T$ models, p_{T} of the boson or the $\not{E}_T$ does not depend strongly on the width of the mediator. An example of the particle-level analysis acceptance using the generator-level cuts from Ref. [**?**] for the photon+$\not{E}_T$ analysis, but raising the photon p_T cut to 150 GeV, is shown in Figure 4, comparing a width that is set to $\Gamma = M_{med}/3$ to the minimal width (the ratio between the two widths ranges from 1.05 to 1.5 with increasing mediator masses).

Acceptance ratio: $\Gamma = \Gamma_{\rm min}$ vs $\Gamma = M_{\rm med}/3$				
	m_χ/GeV			
$M_{\rm med}$/GeV	10	50	200	400
50	0.96	0.99		0.95
100	0.97			
300	1.00	1.02		
600			0.96	
1000	1.01	1.02	1.03	
3000	1.02	1.03		1.01

Table 4: Analysis acceptance ratios for the photon+$\not{E}_T$ analysis when varying the mediator width, in the case of a vector mediator exchanged in the s-channel. The figures shown in this Section have been obtained using a LO UFO model in MadGraph5_aMC@NLO 2.2.3 interfaced to Pythia 8 for the parton shower.

Examples of relevant kinematic distributions for selected benchmark points are shown in Fig. 13.

2.2. Scalar and pseudoscalar mediator, s-channel exchange

In this section, we consider a parallel situation to the vector and axial-vector mediators in the previous sections: a real scalar or a pseudoscalar where the associated scalar is decoupled at higher energies[6]. This section is largely based on Refs. [**? ? ?**] which contain a thorough discussion of these models.

Assuming MFV, spin-0 resonances behave in a similar fashion as the SM Higgs boson. If the mediators are pure singlets of the SM, their interactions with quarks are not $SU(2)_L$ invariant. To restore this invariance, one could include the mixing of such mediators with the Higgs sector. This leads to extra interactions and a more complex phenomenology with respect to what

[6]This assumption does not hold in a UV-complete model where the two components of the complex scalar mediator would be approximately degenerate. The complex scalar case could be studied separately in the case of heavy flavor final states given the sufficiently different kinematics.

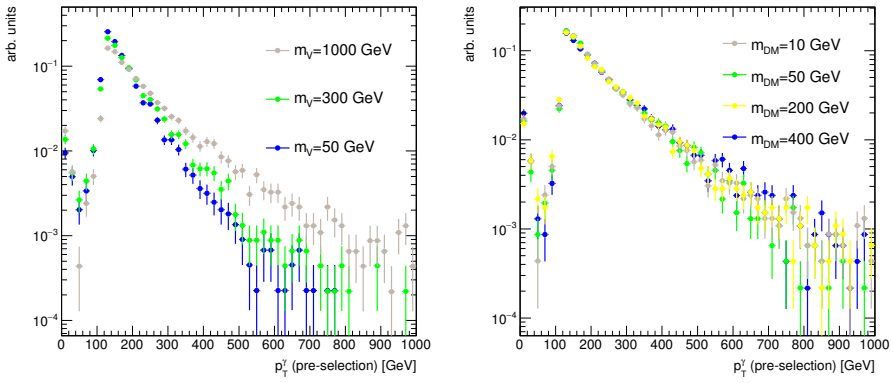

(a) Leading photon transverse momentum distribution for the photon+$\not{E}_T$ final state, for different mediator mass choices, for m_χ =10 GeV.

(b) Leading photon transverse momentum distribution for the photon+$\not{E}_T$ final state, for different DM mass choices, with $M_{\rm med}$ =1 TeV.

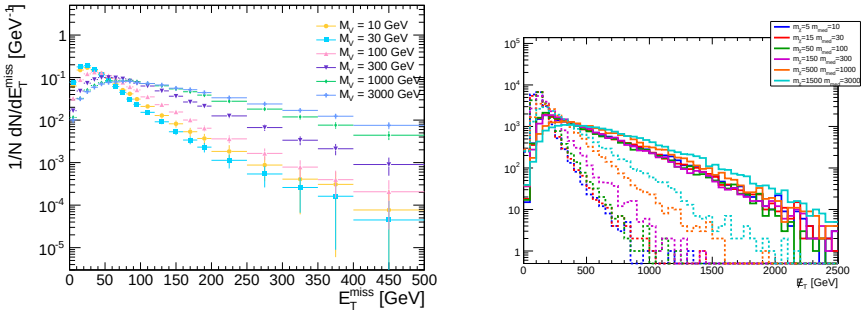

(c) Missing transverse momentum distribution for the leptonic Z+$\not{E}_T$ final state, for different mediator mass choices, for m_χ =15 GeV

(d) Missing transverse momentum distribution for the hadronic W+$\not{E}_T$ final state.

Figure 13: Kinematic distributions relevant for searches with W, Z and photons in the final state, for the simplified model with a vector mediator exchanged in the s-channel.

considered in this Section (for a more complete discussion, see Refs. [**? ?**]). In the interest of simplicity, we do not study models including those interactions in this report as early Run-2 benchmark models, but we give an example of a model of this kind in Appendix **??**.

Relative to the vector and axial-vector models discussed above, the scalar

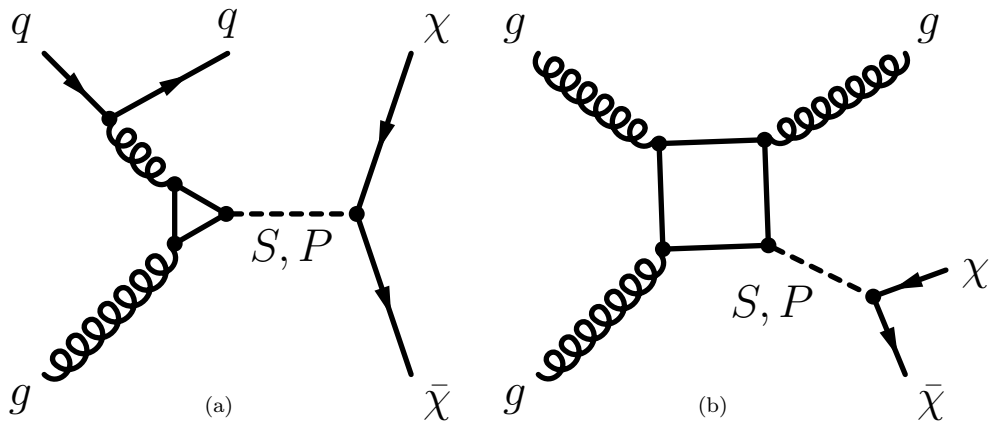

Figure 14: One-loop diagrams of processes exchanging a scalar (S) or pseudoscalar (P) mediator, leading to a mono-jet signature.

models are distinguished by the special consequences of the MFV assumption: the very narrow width of the mediator and its extreme sensitivity to which decays are kinematically available, and the loop-induced coupling to gluons. The interaction Lagrangians are

$$\mathcal{L}_\phi = g_\chi \phi \bar{\chi}\chi + \frac{\phi}{\sqrt{2}} \sum_i \left(g_u y_i^u \bar{u}_i u_i + g_d y_i^d \bar{d}_i d_i + g_\ell y_i^\ell \bar{\ell}_i \ell_i \right) , \tag{6}$$

$$\mathcal{L}_a = i g_\chi a \bar{\chi}\gamma_5\chi + \frac{ia}{\sqrt{2}} \sum_i \left(g_u y_i^u \bar{u}_i \gamma_5 u_i + g_d y_i^d \bar{d}_i \gamma_5 d_i + g_\ell y_i^\ell \bar{\ell}_i \gamma_5 \ell_i \right) . \tag{7}$$

where ϕ and a are respectively the scalar and pseudoscalar mediators, and the Yukawa couplings y_i^f are normalized to the Higgs vev as $y_i^f = \sqrt{2} m_i^f / v$.

The couplings to fermions are proportional to the SM Higgs couplings, yet one is still allowed to adjust an overall strength of the coupling to charged leptons and the relative couplings of u- and d-type quarks. As in the preceding sections, for the sake of simplicity and straightforward comparison, we reduce the couplings to the SM fermions to a single universal parameter $g_\mathrm{q} \equiv g_u = g_d = g_\ell$. Unlike the vector and axial-vector models, the scalar mediators are

allowed to couple to leptons.[7]

The relative discovery and exclusion power of each search can be compared in this framework. However, we again emphasize the importance of searching the full set of allowed channels in case violations of these simplifying assumptions lead to significant modifications of the decay rates that unexpectedly favor different channels than the mix obtained under our assumptions. The coupling g_χ parametrizes the entire dependence on the structure between the mediator and the dark sector.

Given these simplifications, the minimal set of parameters under consideration is

$$\left\{m_\chi,\ m_{\phi/a} = M_{\rm med},\ g_\chi,\ g_{\rm q}\right\}\ . \tag{8}$$

Fig. 14 shows the one-loop diagrams producing a jet+X signature. The full calculation of the top loop is available at LO for DM pair production in association with one parton.

The minimal mediator width (neglecting the small contributions from quarks other than top in the loop) is given by

$$\begin{aligned}\Gamma_{\phi,a} = &\sum_f N_c \frac{y_f^2 g_{\rm q}^2 m_{\phi,a}}{16\pi}\left(1-\frac{4m_f^2}{m_{\phi,a}^2}\right)^{x/2} + \frac{g_\chi^2 m_{\phi,a}}{8\pi}\left(1-\frac{4m_\chi^2}{m_{\phi,a}^2}\right)^{x/2} \\ &+ \frac{\alpha_s^2 g_{\rm q}^2 m_{\phi,a}^3}{32\pi^3 v^2}\left|f_{\phi,a}\left(\tfrac{4m_t^2}{m_{\phi,a}^2}\right)\right|^2\end{aligned} \tag{9}$$

where $x = 3$ for scalars and $x = 1$ for pseudoscalars. The loop integrals, with f as complex functions, are

$$f_\phi(\tau) = \tau\left[1+(1-\tau)\arctan^2\left(\frac{1}{\sqrt{\tau-1}}\right)\right], \tag{10}$$

$$f_a(\tau) = \tau\arctan^2\left(\frac{1}{\sqrt{\tau-1}}\right) \tag{11}$$

where $\tau = 4m_t^2/m_{\phi,a}^2$.

[7] This contribution plays no role for most of the parameter space considered. The choice to allow lepton couplings follows Refs. [? ?].

The minimal widths for scalar and pseudo-scalar mediators with $g_q = g_\chi = 1$ are shown in Fig. 20, illustrating the effect of choosing the SM Higgs-like Yukawa couplings for the SM fermions. For the mediator mass above twice the top quark mass m_t, the minimal width receives the dominant contribution from the top quark. For lighter mediator masses, DM dominates as the couplings to lighter quarks are Yukawa suppressed.

As shown in the diagram of Fig. 14, the lowest order process of these models already involves a one-loop amplitude in QCD, and only LO predictions are currently available. The generator used for the studies for the jet+$\not{E}_T$ signature is POWHEG [? ? ? ? ?], with PYTHIA 8 [?] for the parton shower; within this implementation, the scalar and pseudoscalar mediator benchmark models are known at LO+PS accuracy.

2.2.1. Parameter scan

Similarly as in the case of the vector and axial-vector couplings of spin-1 mediators, scans in the parameter space are performed also for the scalar and pseudo-scalar couplings of the spin-0 mediators in order to decide on the optimized parameter grid for the presentation of Run-2 results. Figures 15- 19 show the scans over the couplings, DM mass and mediator mass and the same conclusions apply as in Section 2.1.

A scan over the mediator mass is shown in Fig. 19 where $M_{\text{med}} = 300$ GeV and 500 GeV are chosen to be below and above $2m_t$. The off-shell case is assumed by taking an extreme limit ($m_\chi = 1$ TeV) in order to study solely the effects of the couplings to quarks. No differences in the kinematic distributions are observed and also the cross sections remain similar in this case. No significant changes appear for mediator masses around the $2m_t$ threshold.

It can be seen in Fig. 21 that the kinematics for the scalar and pseudoscalar models coincides when considering the diagrams in Fig. 14. For this reason, we recommend to fully simulate only one of the two models. No preference is given between the two models as they have the same kinematics, although it is worth noting that the pseudo-scalar model has been used for a DM interpretation of the

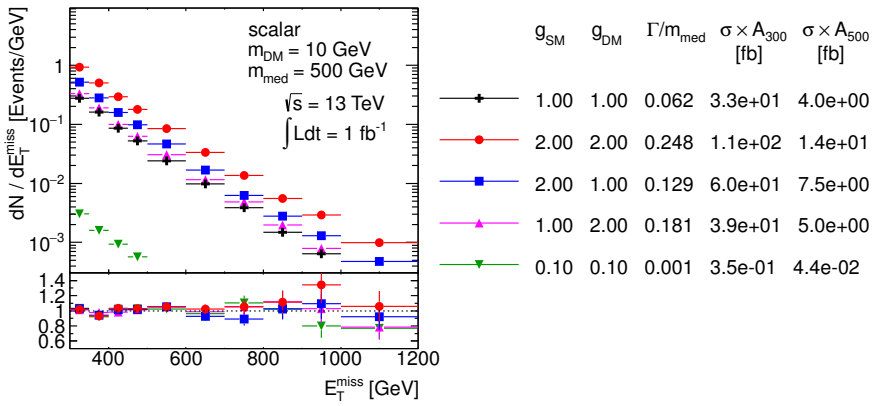

Figure 15: Scan over couplings. The $\not{E}_T$ distribution is compared for the scalar mediator models using the parameters as indicated. Ratios of the normalized distributions with respect to the first one are shown. A_{300} and A_{500} in the table denote the acceptance of the $\not{E}_T >$ 300 GeV and $\not{E}_T > 500$ GeV cut, respectively. Studies in all figures for the jet+$\not{E}_T$ signature is POWHEG, with Pythia 8 for the parton shower;

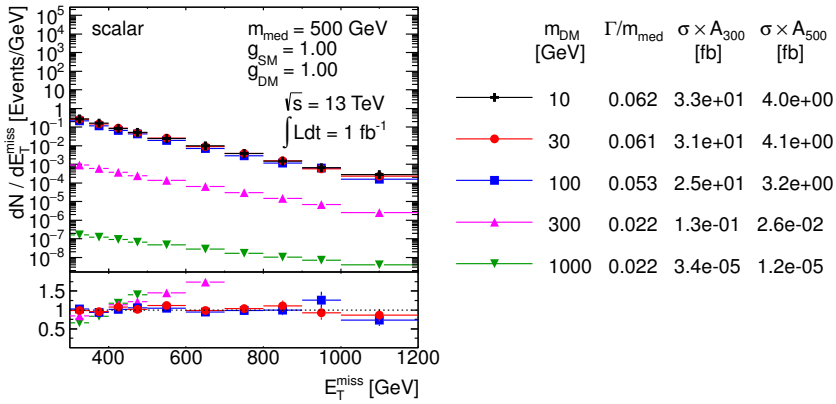

Figure 16: Scan over DM mass. The $\not{E}_T$ distribution is compared for the scalar mediator models using the parameters as indicated. Ratios of the normalized distributions with respect to the first one are shown. A_{300} and A_{500} in the table denote the acceptance of the $\not{E}_T >$ 300 GeV and $\not{E}_T > 500$ GeV cut, respectively.

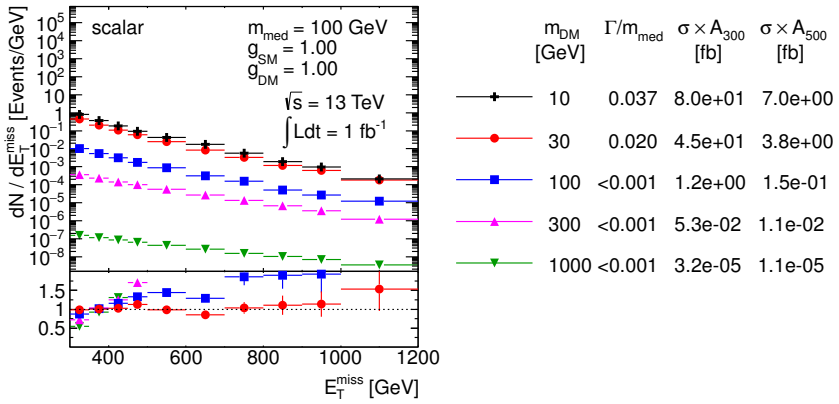

Figure 17: Scan over DM mass. The $\not{E}_T$ distribution is compared for the scalar mediator models using the parameters as indicated. Ratios of the normalized distributions with respect to the first one are shown. A_{300} and A_{500} in the table denote the acceptance of the $\not{E}_T >$ 300 GeV and $\not{E}_T > 500$ GeV cut, respectively.

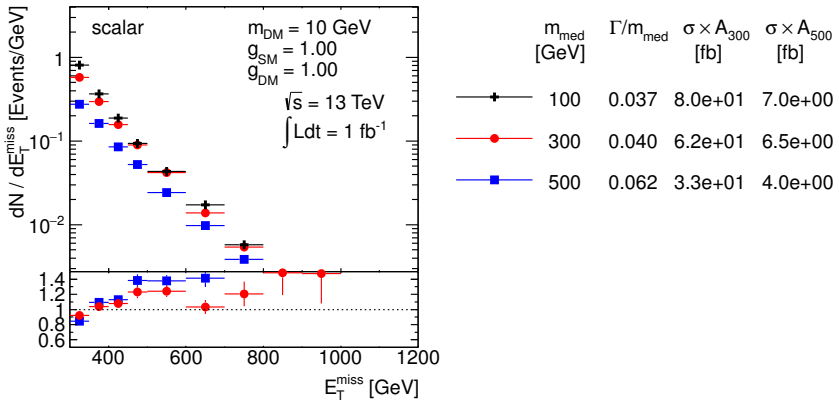

Figure 18: Scan over mediator mass. The $\not{E}_T$ distribution is compared for the scalar mediator models using the parameters as indicated. Ratios of the normalized distributions with respect to the first one are shown. A_{300} and A_{500} in the table denote the acceptance of the $\not{E}_T >$ 300 GeV and $\not{E}_T > 500$ GeV cut, respectively.

DAMA signal and of the galactic center excess [**?**]. Like in the case of the vector and axial-vector models described in Section 2.1.1, the differences between the cross sections for the scalar and pseudo-scalar samples with the same m_χ and M_{med} are increasing with the DM mass for fixed mediator mass, with the pseudo-scalar model yielding larger cross sections. There is an increasing difference between the minimal widths close to the $2m_\chi = M_{\text{med}}$ threshold.

Proposed parameter grid. The optimized parameter grid in the M_{med}–m_χ plane for scalar and pseudo-scalar mediators is motivated by similar arguments as in the previous section. Therefore, a similar pattern is followed here, with the exception of taking $g_{\text{q}} = g_\chi = 1$. The choice of $g_{\text{q}} = 0.25$ for the vector and axial-vector models is motivated by suppressing constraints from di-jets, which is not a concern in the scalar and pseudo-scalar mediator case. Here a di-jet signal emerges only at the 2-loop level through diagrams where the mediator is produced via gluon-gluon fusion and decays back into two gluons through a top loop. The strong loop suppression renders such signals unobservable at the LHC. Further constraints on the scalar and pseudo-scalar mediators may emerge from searches in $t\bar{t}$ final states. Studies of the electroweak effects to $t\bar{t}$ production suggest that one can only expect percent level contributions for $g_{\text{q}} \sim O(1)$ [**?**]. Therefore, keeping $g_{\text{q}} = g_\chi = 1$ is a reasonable choice in the case of the scalar and pseudo-scalar mediators. Contrary to the vector and axial-vector models, note that couplings of 1 lead to $\Gamma_{\text{min}}/M_{\text{med}} \lesssim 0.1$, ensuring the narrow width approximation is applicable. Furthermore, the sensitivity to the highest mediator masses has to be re-evaluated. The generator level cross section times the acceptance at $\not{E}_T > 500$ GeV for the model with couplings $g_{\text{q}} = g_\chi = 1$, light DM of m_χ =10 GeV and a M_{med} =500 GeV scalar mediator is at the order of 10 fb, i.e. just at the edge of the early Run-2 sensitivity. Increasing the mediator mass to 1 TeV pushes the product $\sigma \times A$ down to approximately 0.1 fb, below the LHC sensitivity. Therefore, we choose to remove the 2 TeV mediator mass from the grid and present the final grid with 33 mass points only, as shown in Tab. 5. One point at very high mediator mass (10 TeV) is added for

each of the DM masses scanned, to aid the reinterpretation of results in terms of contact interaction operators (EFTs).

m_χ (GeV)	M_{med} (GeV)								
1	10	20	50	100	200	300	500	1000	10000
10	10	15	50	100					10000
50	10		50	95	200	300			10000
150	10				200	295	500	1000	10000
500	10						500	995	10000
1000	10							1000	10000

Table 5: Simplified model benchmarks for s-channel simplified models (spin-0 mediators decaying to Dirac DM fermions in the scalar and pseudoscalar case, taking the minimum width for $g_{\text{q}} = 1$ and $g_\chi = 1$)

.

For the parameter grid for scalar and pseudo-scalar mediator s-channel exchange, the $\Gamma_{\text{min}}/M_{\text{med}}$ ratio is given in Tables 6 and 7, respectively. In the on-shell regime, the ratio is between 0.04 and 0.1. Very narrow resonances with $\Gamma_{\text{min}}/M_{\text{med}} < 0.001$ correspond to the mass points where the mediator is off-shell. Note that the loop-induced contribution from gluons is ignored in the width calculation.

2.2.2. Additional considerations for $V + \not{E}_T$ signatures

The discussion of parameters for the model with a color-singlet, spin-0 mediator parallels that in Section 2.

Even though the sensitivity of mono-boson searches to this model is low and it may not be in reach of early LHC searches, this model can be generated for W, Z and photon searches in order to reproduce the kinematics of contact interaction operators that are further described in Section **??**, to aid later reinterpretation.

Other models of DM that couple dominantly to electroweak gauge bosons through either pseudo-scalar or vector mediators can be found in Ref. [**?**].

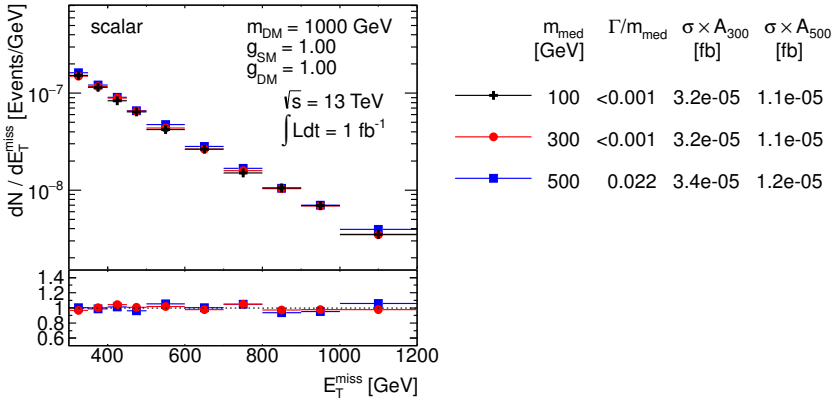

Figure 19: Scan over mediator mass. The $\not{E}_T$ distribution is compared for the scalar mediator models using the parameters as indicated. Ratios of the normalized distributions with respect to the first one are shown. A_{300} and A_{500} in the table denote the acceptance of the $\not{E}_T > 300$ GeV and $\not{E}_T > 500$ GeV cut, respectively.

m_χ/ GeV	M_{med}/ GeV								
	10	20	50	100	200	300	500	1000	10000
1	0.040	0.040	0.040	0.040	0.040	0.040	0.062	0.089	0.099
10	<0.001	<0.001	0.040	0.040					0.099
50	<0.001		<0.001	<0.001	0.040	0.040			0.099
150	<0.001				<0.001	<0.001	0.062	0.089	0.099
500	<0.001						0.022	0.049	0.099
1000	<0.001							0.049	0.099

Table 6: Minimal width of the scalar mediator exchanged in s-channel divided by its mass, assuming $g_q = g_\chi = 1$. The loop-induced gluon contribution is ignored. The numbers tabulated under $2m_\chi = M_{\text{med}}$ correspond to the width calculated for $M_{\text{med}} - 5$ GeV.

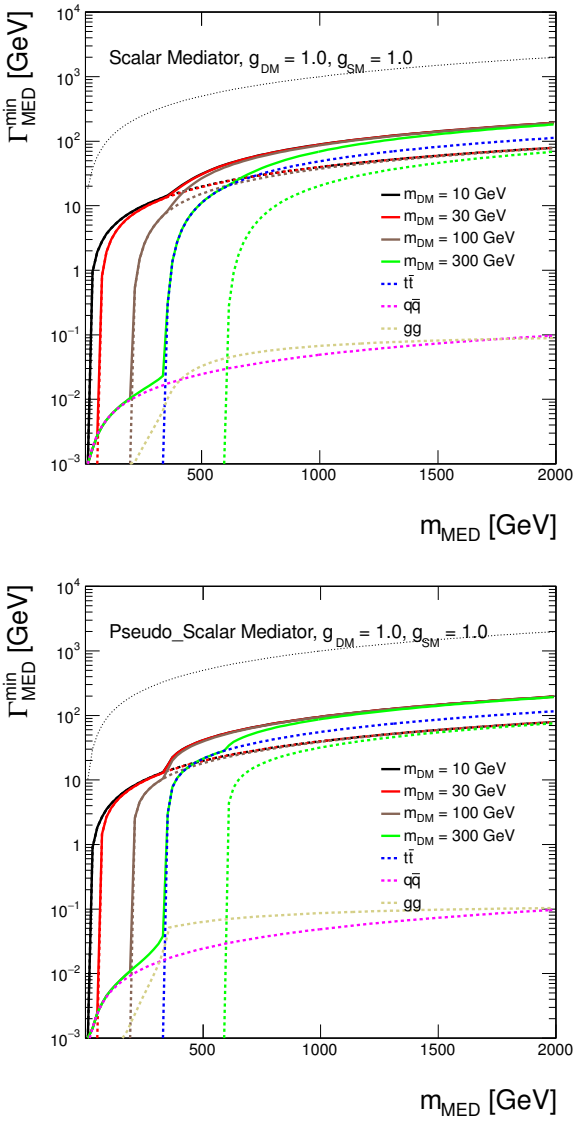

Figure 20: Minimal width as a function of mediator mass for scalar and pseudo-scalar mediator assuming couplings of 1. The total width is shown as solid lines for DM masses of m_χ =10 GeV, 30 GeV, 100 GeV and 300 GeV in black, red, brown and green, respectively. The individual contributions from DM are indicated by dotted lines with the same colors. The contribution from all quarks but top is shown as magenta dotted line and the contribution from top quarks only is illustrated by the dotted blue line. The dotted beige line shows the contribution from the coupling to gluons. The dotted black line shows the extreme case $\Gamma_{\rm min} = M_{\rm med}$.

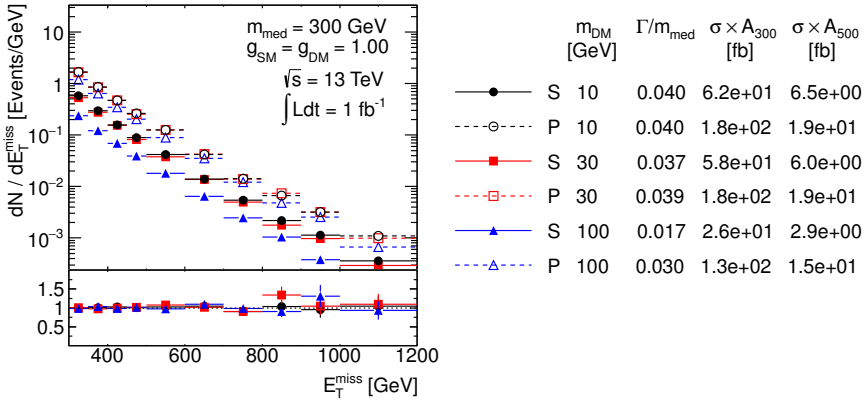

Figure 21: Comparison of the $\not{E}_T$ distributions for the scalar and pseudoscalar models for different $M_{\text{med}} = 300$ GeV and different DM masses. Ratios of the normalized distributions with respect to the first one are shown. A_{300} and A_{500} in the table denote the acceptance of the $\not{E}_T > 300$ GeV and $\not{E}_T > 500$ GeV cut, respectively.

m_χ/ GeV	M_{med}/ GeV								
	10	20	50	100	200	300	500	1000	10000
1	0.040	0.040	0.040	0.040	0.040	0.040	0.083	0.095	0.099
10	<0.001	<0.001	0.040	0.040					0.099
50	<0.001		<0.001	<0.001	0.040	0.040			0.099
150	<0.001				<0.001	<0.001	0.083	0.095	0.099
500	<0.001						0.043	0.056	0.099
1000	<0.001							0.056	0.099

Table 7: Minimal width of the pseudo-scalar mediator exchanged in s-channel divided by its mass, assuming $g_{\text{q}} = g_\chi = 1$. The loop-induced gluon contribution is ignored. The numbers tabulated under $2m_\chi = M_{\text{med}}$ correspond to the width calculated for $M_{\text{med}} - 5$ GeV.

2.2.3. Additional considerations for $t\bar{t}$ and $b\bar{b}$+$\not{E}_T$ signatures

With the MFV assumption, the top and bottom quark can play an important role in the phenomenology. The scalar and pseudoscalar mediator models predict not only the monojet process described in Section 2.2, but also production of Dark Matter in association with top (or bottom) pairs, as illustrated in Fig. 22. Dedicated searches including jets from heavy flavor quarks in the final state can be designed for this signature. Another class of simplified models, which includes a Dark Matter interpretation among many others, and yields a single top quark in the final state, is detailed in Appendix **??**.

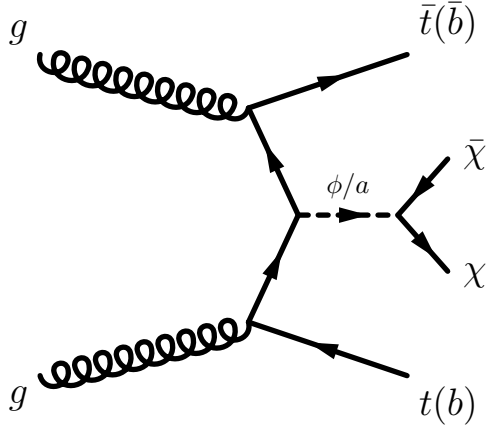

Figure 22: Representative Feynman diagram showing the pair production of Dark Matter particles in association with $t\bar{t}$ (or $b\bar{b}$).

In addition to the $t\bar{t}$+DM models illustrated in Fig. 22, some theoretically motivated scenario (e.g. for high $tan\beta$ in 2HDM in the pMSSM) privilege the coupling of spin-0 mediators to down generation quarks. This assumption motivates the study of final states involving b-quarks as a complementary search to the $t\bar{t}$+DM models, to directly probe the b-quark coupling. An example of such a model can be found in Ref. [**?**] and can be obtained by replacing top quarks with b quarks in Fig. 22. Note that, because of the kinematics features of b quark production relative to heavy t quark production, a $b\bar{b}$+DM final state may only yield one experimentally visible b quark, leading to a mono-b signature in a model that conserves b flavor.

Dedicated implementations of these models for the work of this Forum are available at LO+PS accuracy, even though the state of the art is set to improve on a timescale beyond that for early Run-2 DM searches as detailed in Section **??**. The studies in this Section have been produced using a leading order UFO model within MadGraph5_aMC@NLO 2.2.2 [**? ? ?**] using Pythia 8 for the parton shower.

Parameter scan. The parameter scan for the dedicated $t\bar{t}$+$\not{E}_T$ searches has been studied in detail to target the production mechanism of DM associated with heavy flavor quarks, and shares many details of the scan for the scalar model with a gluon radiation. The benchmark points scanning the model parameters have been selected to ensure that the kinematic features of the parameter space are sufficiently represented. Detailed studies were performed to identify points in the m_χ, $m_{\phi,a}$, g_χ, g_q (and $\Gamma_{\phi,a}$) parameter space that differ significantly from each other in terms of expected detector acceptance. Because missing transverse momentum is the key observable for searches, the mediator p_T spectra is taken to represent the main kinematics of a model. Another consideration in determining the set of benchmarks is to focus on the parameter space where we expect the searches to be sensitive during the 2015 LHC run. Based on a projected integrated luminosity of $30\,\mathrm{fb}^{-1}$ expected for 2015, we disregard model points with a cross section times branching ratio smaller than 0.1 fb, corresponding to a minimum of one expected event assuming a 0.1% efficiency times acceptance.

The kinematics is most dependent on the masses m_χ and $m_{\phi,a}$. Figure 23 and 24 show typical dependencies for scalar and pseudoscalar couplings respectively. Typically, the mediator p_T spectrum broadens with larger $m_{\phi,a}$. The kinematics are also different between on-shell ($M_\mathrm{med} > 2m_\chi$) and off-shell ($M_\mathrm{med} < 2m_\chi$) mediators as discussed in Section 2.2. Furthermore, the kinematic differences in the $\not{E}_T$ spectrum between scalar and pseudoscalar are larger for light mediator masses with respect to heavier mediators. It is therefore important to choose benchmark points covering on-shell and off-shell mediators with sufficient granularity, including the transition region between on-shell and

off-shell mediators.

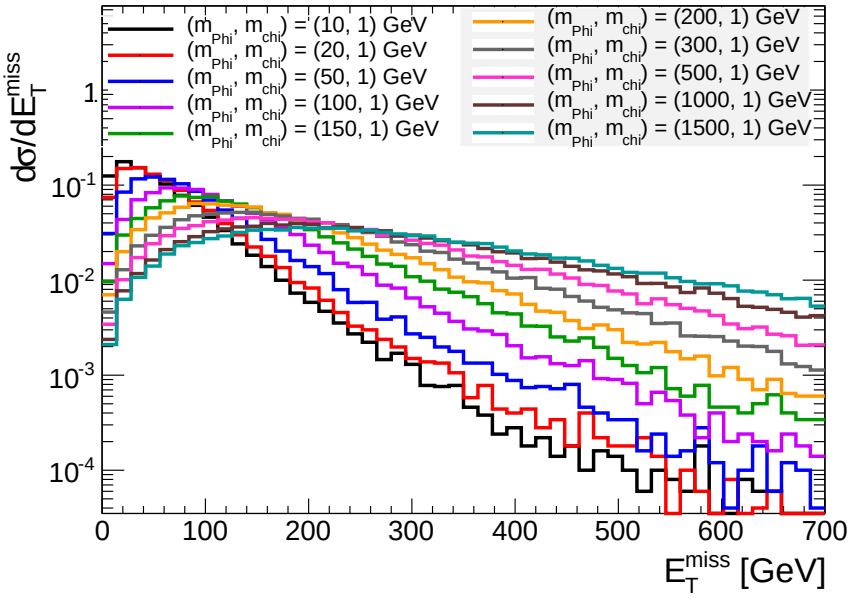

Figure 23: Example of the dependence of the kinematics on the scalar mediator mass in the $t\bar{t}$+$\not{E}_T$ signature. The Dark Matter mass is fixed to be m_χ =1GeV.

Typically only weak dependencies on couplings are observed (see Fig 25) where the variation with width of the integral over parton distributions is unimportant. As shown in Section 2.1.1, for couplings $\sim O(1)$ the width is large enough that the p_T of the mediator is determined mainly by the PDF.

At large mediator masses ($\sim$ 1.5 TeV) or very small couplings ($\sim 10^{-2}$), width effects are significant, but these regimes have production cross sections that are too small to be relevant for 30 fb^{-1} and are not studied here. However, with the full Run 2 dataset, such models may be within reach.

Another case where the width can impact the kinematics is when $m_{\phi,a}$ is slightly larger than $2m_\chi$. Here, the width determines the relative contribution between on-shell and off-shell mediators. An example is given in Fig. 26. As the minimal width choice pursued in this document is the most conservative one, this effect can be neglected in order to reduce the number of benchmark points

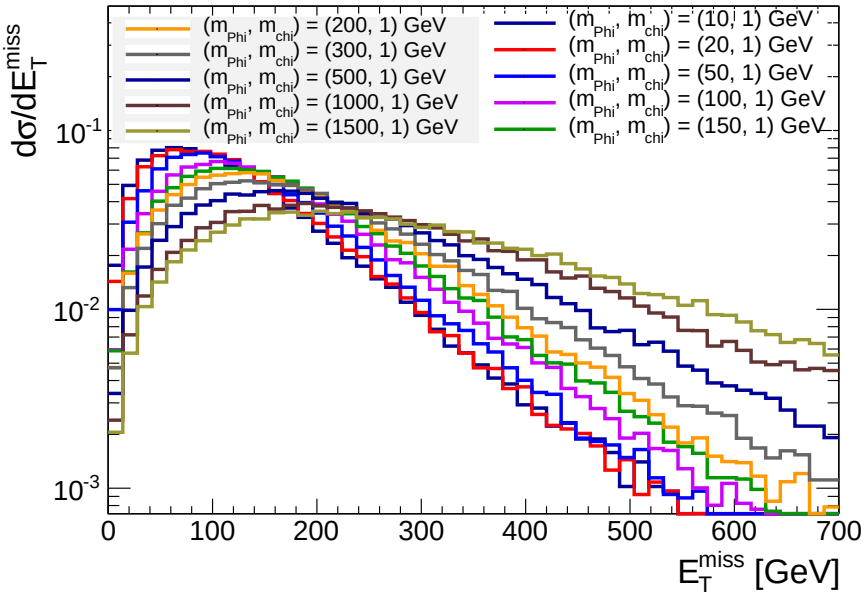

Figure 24: Example of the dependence of the kinematics on the pseudoscalar mediator mass in the $t\bar{t}$+$\not{E}_T$. The Dark Matter mass is fixed to be m_χ =1GeV. All figures concerning the $t\bar{t}$+$\not{E}_T$ signature have been produced using a leading order model within MadGraph5_aMC@NLO 2.2.2, using Pythia 8 for the parton shower.

to be generated.

The points for the parameter scan chosen for this model are listed in Table 5, chosen to be harmonized with those for other analyses employing the same scalar model as benchmark. Based on the sensitivity considerations above, DM masses are only simulated up to 500 GeV (but the 5 TeV mediator point is retained) leading to a total of 24 benchmark points. However for these searches we recommend to generate and simulate scalar and pseudoscalar models separately, as the kinematics differs due to the different coupling of the mediator to the final state top quarks in the two cases, as shown in Figs. 23 and 24.

Similar studies were performed in the $b\bar{b}$ case. It was found that they show the same weak dependence of the kinematics of the event on the mediator width. The same benchmark parameters of the $t\bar{t}$ case could then be chosen.

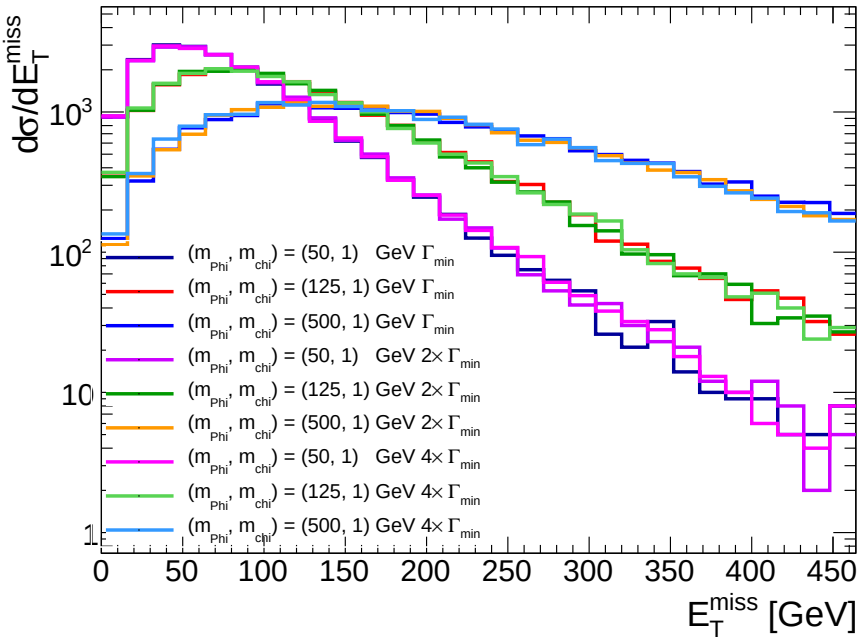

Figure 25: Study of the dependence of kinematics on the width of a scalar mediator $t\bar{t}+\not{E}_T$. The width is increased up to four times the minimal width for each mediator and Dark Matter mass combination.

2.3. Colored scalar mediator, t-channel exchange

The preceding sections address models with a Dirac fermion coupled to the SM through exchange of a neutral spin-0 or spin-1 particle in an s-channel process. A t-channel process may couple the SM and DM directly, leading to a different phenomenology. For completeness, we examine a model where χ is a Standard Model (SM) singlet, a Dirac fermion; the mediating particle, labeled ϕ, is a charged scalar color triplet and the SM particle is a quark. Such models have been studied in Refs. [**? ? ? ? ? ?**]. However, these models have not been studied as extensively as others in this Forum.

Following the example of Ref. [**?**], the interaction Lagrangian is written as

$$\mathcal{L}_{\text{int}} = g \sum_{i=1,2} (\phi_{(i),L} \bar{Q}_{(i),L} + \phi_{(i),u,R} \bar{u}_{(i),R} + \phi_{(i),d,R} \bar{d}_{(i),R}) \chi \qquad (12)$$

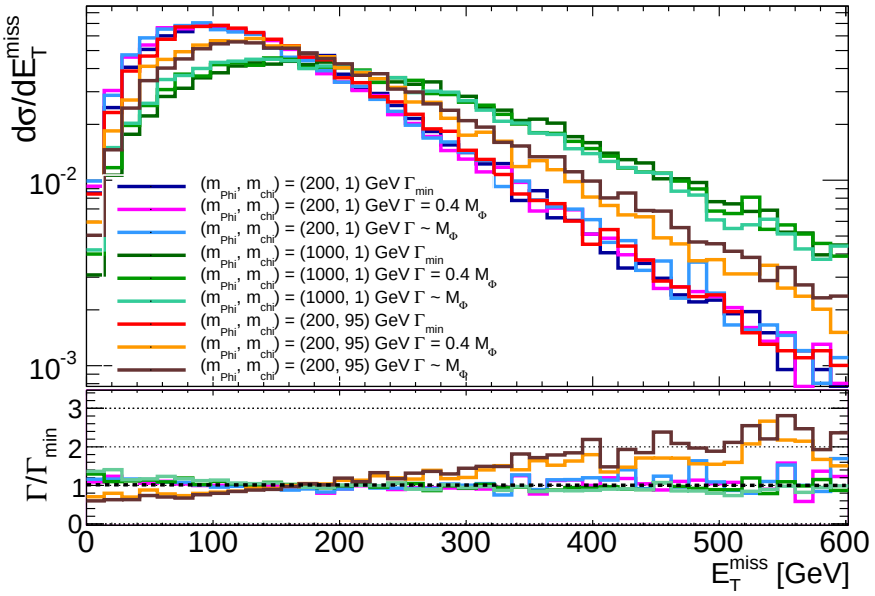

Figure 26: Dependence of the kinematics on the width of a scalar mediator $t\bar{t}$+$\not{E}_T$. The width is increased up to the mediator mass. Choices of mediator and Dark Matter masses such that $m_{\phi,a}$ is slightly larger than $2m_\chi$ is the only case that shows a sizeable variation of the kinematics as a function of the width.

where $Q_{(i),L}$, $u_{(i),R}$ and $d_{(i),R}$ are the SM quarks of the i-th generation and $\phi_{(i),L}$, $\phi_{(i),u,R}$ and $\phi_{(i),d,R}$ are the corresponding mediators, which (unlike the s-channel mediators) must be heavier than χ. These mediators have SM gauge representations under $(SU(3), SU(2))_Y$ of $(3,2)_{-1/6}$, $(3,1)_{2/3}$ and $(3,1)_{-1/3}$ respectively. Variations of the model previously studied in the literature include coupling to the left-handed quarks only [**?** **?**], to the $\phi_{(i),u,R}$ [**?**] or $\phi_{(i),d,R}$ [**?** **?**], or some combination [**?** **?**].

The minimal width of each mediator is expressed, using the example of decay

to an up quark, as

$$\Gamma(\phi_{(i)} \to \bar{u}_{(i)}\chi) = \frac{g_{(i)}^2}{16\pi M_{\phi_{(i)}}^3}(M_{\phi_{(i)}}^2 - m_{u_{(i)}}^2 - m_\chi^2) \times \sqrt{(M_{\phi_{(i)}}^2 - (m_{u_{(i)}} + m_\chi)^2)(M_{\phi_{(i)}}^2 - (m_{u_{(i)}} - m_\chi)^2)}\,, \tag{13}$$

which reduces to

$$\frac{g_{(i)}^2 M_{\phi_{(i)}}}{16\pi}\left(1 - \frac{m_\chi^2}{M_{\phi_{(i)}}^2}\right)^2 \tag{14}$$

in the limit $M_{\phi_{(i)}}, m_\chi \gg m_{u_{(i)}}$.

The generation index i for $\phi_{(i)}$ is linked to the incoming fermion(s), and it runs on all three quark generations due to the MFV assumption. Ref. [**?**] considers two extreme cases for this model in terms of cross-sections: the case in which all mediator flavors are present, leading to the maximal cross-section, and the case in which only right-handed down-type mediators are present. Neither of the models in this reference include couplings to the third quark generation, leading to a violation of the MFV assumption. In the case of purely down-type right-handed squarks this is still safe from flavor constraints. Furthermore, reintroducing the third generation squarks would lead to models that produce qualitatively similar signals in the mono-jet and SUSY squark searches, the main difference being the production cross-section. At the same time the presence of third generation squarks will lead to further constraints from other searches such as those for mono-bjets, for stops and for sbottoms, as discussed in Sec. 2.4. The studies in this Section are performed using a model with a mediator coupling to all three generation, following Ref. [**?**]. Further differences between the two models (hypercharge, chirality) only lead to a change in the cross-section. The LO UFO model is interfaced to MadGraph5_aMC@NLO v2.2.3, but it was not possible to go beyond parton-level studies and interface those models to a parton shower in time for the conclusion of this Forum. The state of the art for calculating these models is LO+PS, and the implementation of multi-parton merging has been studied in detail [**? ? ? ?**], and further studies should be

undertaken prior to generating signal samples for early Run-2 LHC searches.

The leading-order processes involved in $\not{E}_T$+jet production are shown in Fig. 27. This model can also give a signal in the $\not{E}_T$ + di-jet channel when, for example, the χ is exchanged in the t-channel and the resulting ϕ pair each decay to a jet + χ. Fig. 28 shows the leading order diagrams. Except for the gg induced process, di-jet production through the third-generation mediator $\phi_{(3),u}$ is not possible, and production through $\phi_{(3),d}$ is suppressed. However, if the coupling g includes a Yukawa coupling proportional to the quark mass, and g is sufficiently large, LHC searches will still be sensitive to this model, as explained in Section 2.4.

The diagram involving the t-channel exchange of χ is strongly dependent upon the Dirac fermion assumption. For a Majorana fermion, $q\bar{q}, \bar{q}\bar{q}$, and qq production would be possible with the latter having a pronounced enhancement at the LHC.

This model is similar to the simplified model considered in SUSY searches, implemented as the MSSM with only light squarks and a neutralino, except for two distinct points: the χ is a Dirac fermion and the coupling g is not limited to be weak scale ($g \ll 1$). In the MSSM, most of these processes are sub-dominant, even if resonantly enhanced, because the production is proportional to weak couplings. In the more general theories considered here, g is free to take on large values of order 1 or more, and thus diagrams neglected in MSSM simulation can occur at a much higher rate here. While constraints from SUSY jets+$\not{E}_T$ analyses on MSSM models can be recast to apply to the specific model in this report, DM searches should also directly test their sensitivity to the MSSM benchmark models.

The state of the art calculation for these models is LO and they can be interfaced with a parton shower program. The studies in this Section use a LO model implementation within MadGraph5_aMC@NLO v2.2.3, but no parton shower could be employed in the time-frame of the conclusions of this Forum. Further implementation details can be found in Section **??**.

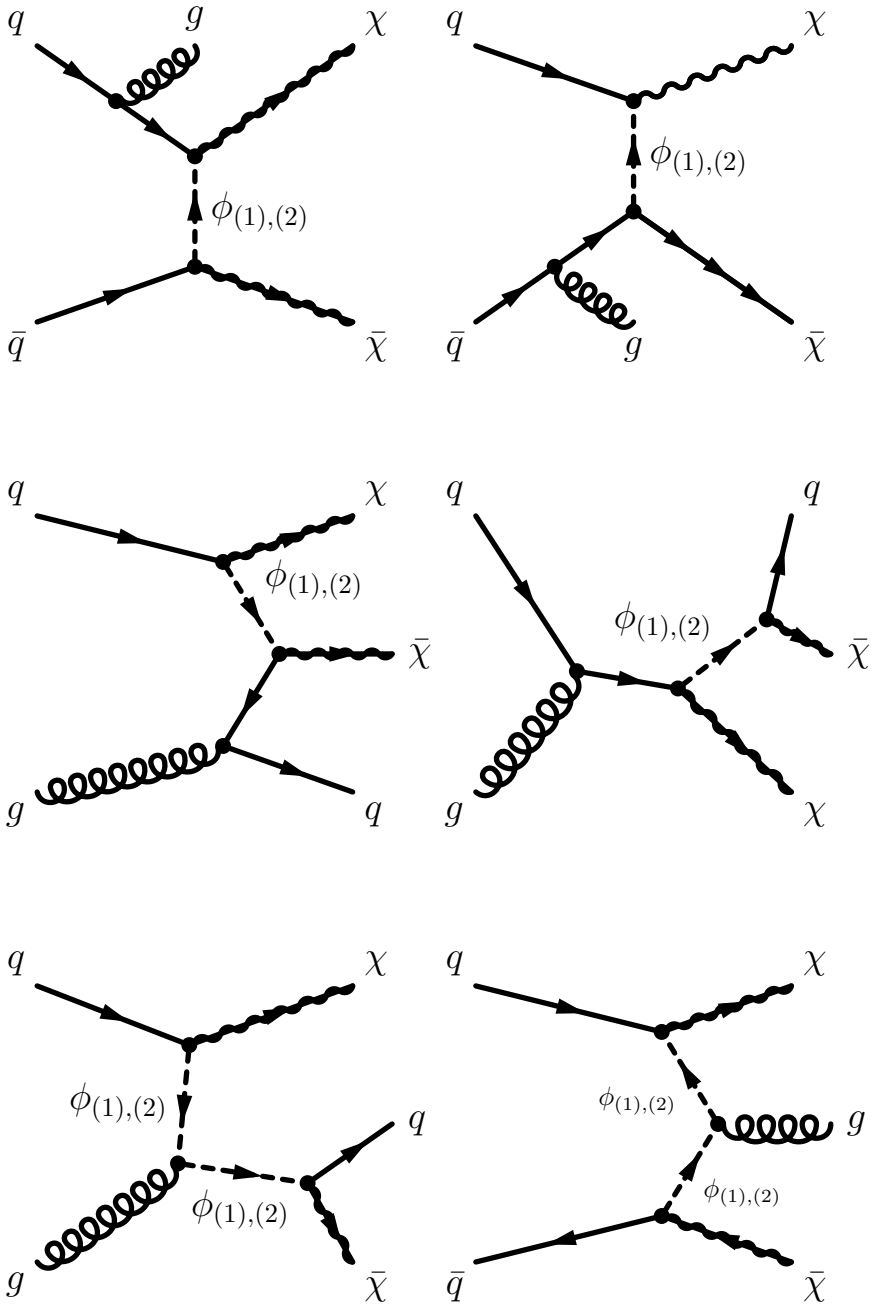

Figure 27: Leading order mono-jet t-channel processes, adapted from [**?**].

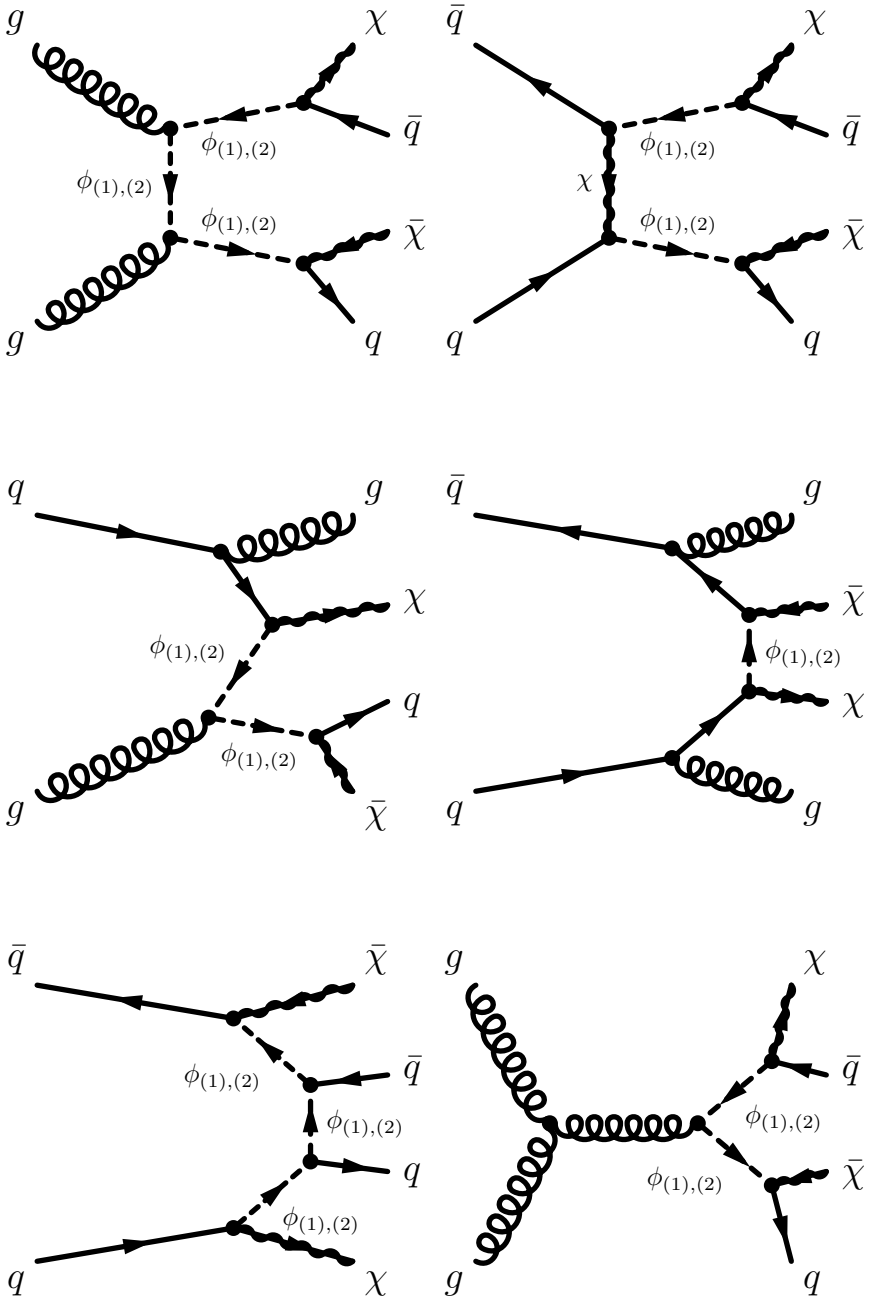

Figure 28: Leading order two-jet t-channel processes, adapted from [**?**].

2.3.1. Parameter scan

As for the s-channel models, we adopt the simplifying assumption that the mediator masses and couplings are equal for each flavor and handedness. The free parameters are then

$$\{m_\chi,\, M_\phi,\, g\}. \tag{15}$$

Ref. [**?**] studies the parameter space and obtains bounds on this model from LHC Run-1 mono-jet and dijets+$\not{E}_T$ data. The Forum did not exhaustively compare the kinematic distributions of the t-channel models as done in the s-channel case. In particular, the absence of a parton shower simulation can affect some of the conclusions on the points and sensitivity chosen. While this means the conclusions on the parameter scan below should be taken with more caution, the model is plausible and distinctive, and it should be included in the design of early Run-2 LHC searches.

As in the s-channel models, scans should be performed over m_χ and M_ϕ. The viable ranges of both parameters nearly coincide with the scan proposed for the s-channel. For the early Run-2 searches, we recommend to generate and fully simulate a subset of the s-channel mono-jet grid that accounts for the on-shell and off-shell regions. In contrast to the s-channel case, the bounds one obtains from $\not{E}_T$+X searches depend strongly on the width of the mediator, as is visible in Figs. 5 and 6 of Ref. [**?**] and in Fig. 29 (a), except in the heavy mediator limit ($M_\phi \approx 2\,\text{TeV}$). This figure has been obtained applying a simplified analysis selection (cuts on the leading jet p_T >150 GeV and $\eta < 2.8$, $\not{E}_T$>150 GeV.) using MadAnalysis [**? ?**]. Figure 29 (b) also shows that, if the DM mass is low and the mediator is produced on-shell and its width is narrow, the cross-section is dominated by $qg \to q\chi\chi$ diagram. The mediator energy is then split evenly between the light DM particles and the quark, leading to a broad enhancement at $M_\text{med}/2$.

Points with distinct kinematic distributions for a preliminary scan in { m_χ, M_ϕ, g} are selected taking into account the expected sensitivity of Run-2

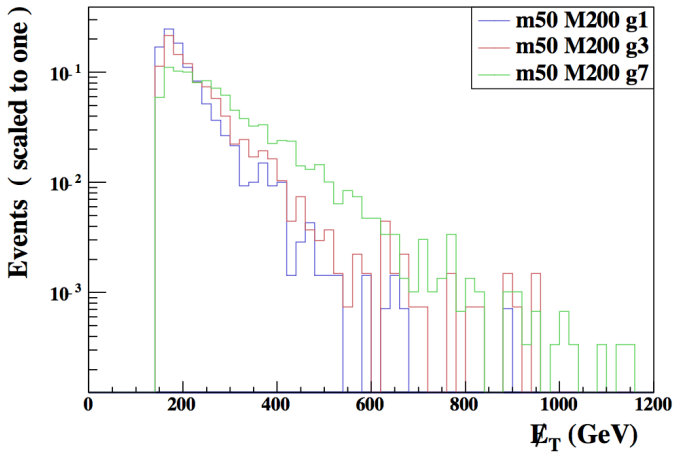

(a) $\not{E}_T$ distribution for a 200 GeV t-channel mediator, when varying the couplings.

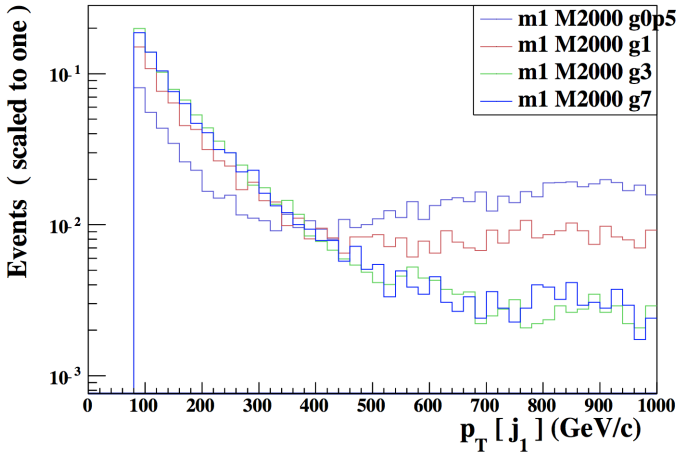

(b) Leading jet p_{T} distribution for a 2 TeV t-channel mediator with small (g=0.5) to large (g=7) couplings with a DM mass of 1 GeV

Figure 29: [

14pt]Kinematic distributions normalized to unit area from the t-channel model from Ref. [**?**], using MadAnalysis [**? ?**] and simplified analysis cuts on the leading jet p_{T} >150 GeV and $\eta < 2.8$, $\not{E}_T$>150 GeV. For these models, a LO UFO model is interfaced to MadGraph5_aMC@NLO v2.2.3, and studies are at parton-level only.

searches, and requiring at least 100 events to pass the kinematic cuts outlined for Fig. 29 in 25 fb^{-1} of collected data, and respect $\Gamma/M_{\text{med}} < 1$. They are outlined in Table 8. The conclusions in this table may change when a parton shower is employed together with multiparton matching.

m_χ/ GeV	M_{med}/ GeV							couplings
1	10	50	100	300				0.1, 1, 3, 7
1					500	1000		0.25, 1, 3, 7
1							2000	1, 3, 7
50		55						0.1, 1, 3, 4π
50			200	300				0.1, 1, 3, 7
500					550			1, 3
500						1000		0.25, 1, 3
500							2000	3
1000						1100		3, 4π
1000							2000	3

Table 8: Simplified model benchmark points for t-channel simplified model (spin-0 mediators coupling to Dirac DM fermions, taking the minimum width.)

.

2.3.2. Additional considerations for $V + \not{E}_T$ signatures

The models and parameters with emission of an EW boson generally follow those in Section 2.3. even though different diagrams are involved. A representative Feynman diagram can be constructed by replacing a final-state gluon in Fig. 27 with a γ, W, Z boson, but radiation of electroweak bosons directly from the mediator also leads to a mono-boson signature.

The models considered in Section 2.3 present a relevant difference concerning final states with an electroweak boson. In the model in [**?**], both right- and left-handed mediators can radiate a Z boson, while only the left-handed mediator in [**?**] allows for W and Z radiation.

The studies in this Section use the LO+PS UFO model from [**?**] in MadGraph5_aMC@NLO v2.2.3, using Pythia 8 for the parton shower. Figure 30 shows the $\not{E}_T$ distribution for the hadronic Z+$\not{E}_T$ final state, with varying DM and mediator mass, before any selection. The acceptance for a series of basic analysis selections ($\not{E}_T$ >350 GeV, leading jet p_T > 40 GeV, minimum azimuthal angle between jet and $\not{E}_T$ > 0.4) applied at the generator level is shown in Figure 31.

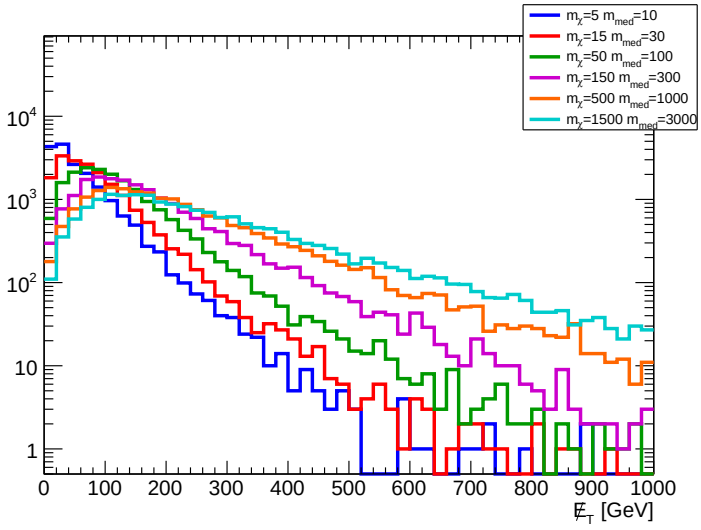

Figure 30: Missing transverse momentum distribution for the hadronic Z+$\not{E}_T$ final state, for the simplified model with a colored scalar mediator exchanged in the t-channel.

The discussion of the parameter scan for the t-channel model in the case of signatures including EW bosons parallels that of the monojet case for mediator and DM masses, but no kinematic dependence on the width is observed, so a coupling scan is not needed.

2.4. Additional considerations for signatures with b−quarks + $\not{E}_T$

Models of bottom-flavored Dark Matter that are closely related to the t-channel mediated model from this Section have been proposed in Refs. [**? ?**]. We de-

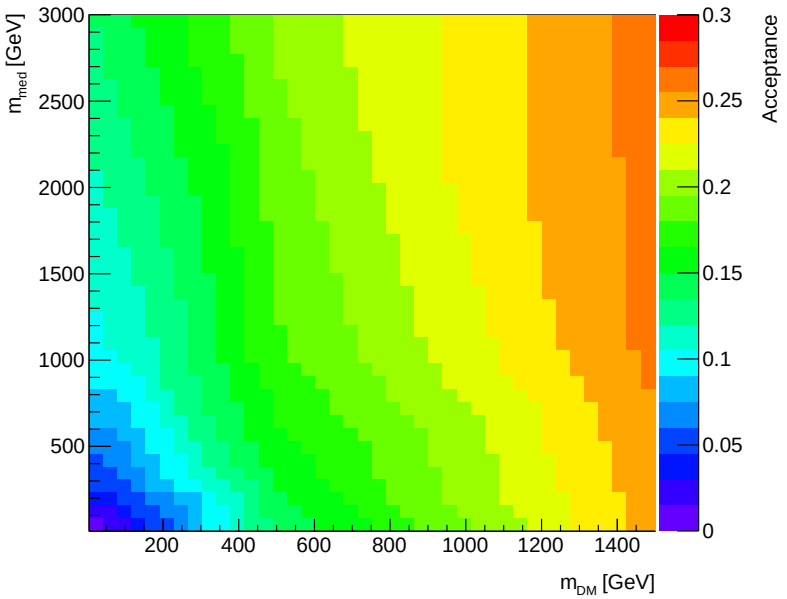

Figure 31: Acceptance for the hadronic Z+$\not{E}_T$ final state, for the simplified model with a colored scalar mediator exchanged in the t-channel.

scribe the b-FDM model of Ref. [**?**], created to explain the Galactic Center (GC) gamma-ray excess observed in data collected by the Fermi-LAT collaboration [**?** **?**]. This model favors couplings to third-generation quarks via Yukawa couplings, therefore respecting the MFV assumption.

The model contains a Dirac fermion transforming as a flavor triplet, exclusively coupling to right-handed down-type quarks. The third component of the triplet χ_b comprises the cosmological DM. Within the MFV framework, the other fermions in the flavor triplet can be made sufficiently heavy and weakly-coupled that they can be neglected in the analysis. A flavor singlet, color triplet scalar field Φ mediates the interactions between the DM and the Standard Model quarks. The model is similar to the MSSM with a light bottom squark and neutralino, and is thus a flavor-specific example of a t-channel model. Similar top-flavored models can exist, as e.g. in Refs. [**?** **?**]. In the case where the top coupling is the main DM coupling, the signal is very similar to a signal from a

stop quark, since unlike the other t-channel cases there is no top in the initial state parton distribution functions (PDFs). This is the reason why it wasn't considered as an additional model. More recent literature shows that other flavor states could also contribute to LHC signals, as shown in Ref. [**?**], but such models will have to be investigate on a longer timescale with respect to that of this Forum.

The Lagrangian considered is given by

$$-\mathcal{L} \supset g\Phi^* \bar{\chi}_b b_R + \text{h.c.} \tag{16}$$

This model is known at LO+PS accuracy, and the studies in this Section use a LO model implementation within MadGraph5_aMC@NLO v2.2.3 interfaced to Pythia 8 for the parton shower. Further implementation details can be found in Section **??**.

Parameter scan. In this model, the interference of diagrams with QCD production of the mediator (which scale as g_s^2) with diagrams that are proportional to the coupling g in the b+$\not{E}_T$ and $b\bar{b}$+$\not{E}_T$ final states. In the case of large couplings, this is not conducive to a simple scaling behavior that would allow us to reduce the number of points to be simulated. This can be seen in Fig. 33.

A full study of the parameter scan for this model was not available for this report; thus for early Run-2 searches we recommend scanning a range of possible widths as discussed in a more limited way than for the t-channel monojet, spanning from the minimal width to a value approaching the particle limit, e.g. $g = 0.5, 1, 2, 3$. A coupling benchmark such as $g = 1$ should be considered for each mass point since this would be a distinctive feature of this benchmark from SUSY models with sbottom squarks (see Section 2.3 for further discussion).

A scan of Dark Matter and mediator masses should be done in the on-shell region $M_\Phi > m_\chi + m_b$, since the cross-sections in the off-shell region are too small to be probed with early LHC data, spanning from 10 to 500 GeV in m_χ and from 10 to 1300 GeV in M_Φ. Examples of the kinematic distributions produced

by this model are shown in Fig. 32 [8].

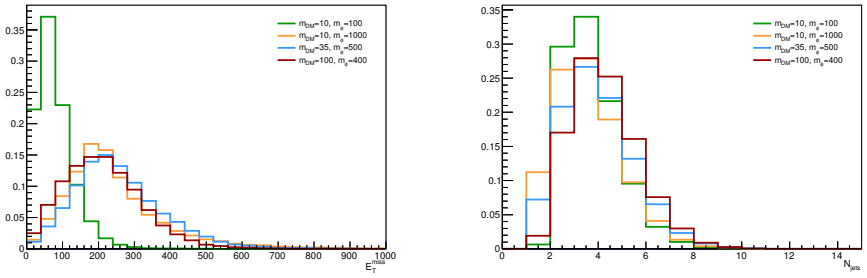

Figure 32: $\not{E}_T$ (left) and jet multiplicity (right) for various DM and mediator masses and couplings normalized to the relic density observed in the early universe. Studies in this section use a LO UFO model implementation within MadGraph5_aMC@NLO v2.2.3 interfaced to Pythia 8 for the parton shower.

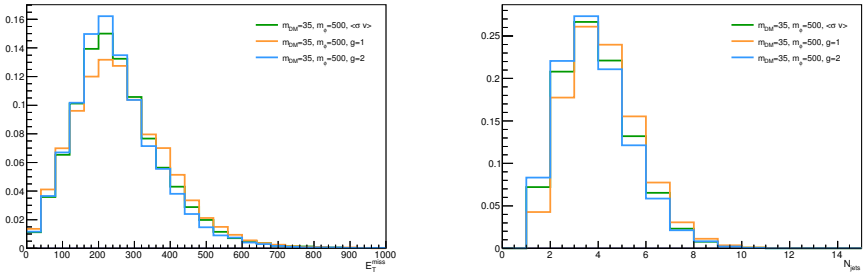

Figure 33: $\not{E}_T$ (left) and jet multiplicity (right) for $m_\chi = 35$ GeV and $M_\Phi = 500$ GeV for varying couplings of $g = 1, 2$

3. Spin-2 mediator

In models with extra dimensions, the Kaluza-Klein excitations of the graviton could also serve as a mediator between the SM and dark sector physics. This kind of model was not studied in the forum and is not included in the

[8] Following the grounding assumptions in this report, the normalization to the relic density is considered only in these example plots rather than as a necessary ingredient for the parameter scan of this model.

recommendations, but models such as Ref. [**?** **?**] may warrant further study on a longer timescale.

4. Presentation of results for reinterpretation of *s*-channel mediator models

The aim of the parameter grid optimization done for the s-channel models in the previous sections is to reduce the parameter space that must be simulated. We then need a procedure for populating the full parameter space by using the simulated grid points. We recommend doing this as follows:

- When the dependences on parameters are known, the cross sections and efficiencies at general points can be calculated from the grid data.
- In other cases, this information can be obtained by interpolation between the grid points. We have chosen the grid points so that the dependence is sufficiently smooth that this will be possible.

The results of the scan over the couplings presented in the previous sections indicate that there are no changes in kinematic distributions for different choices of the coupling strengths. This means that the acceptance remains the same in the whole g_{q}–g_{χ} plane and it is sufficient to perform the detector simulation only for one single choice of g_{q}, g_{χ}. The resulting truth-level selection acceptance and the detector reconstruction efficiency can then be applied to all remaining grid points in the g_{q}–g_{χ} plane where only the generator-level cross section needs to be known. This significantly reduces the computing time as the detector response is by far the most CPU-intensive part of the Monte Carlo sample production. However, the number of generated samples can be reduced even further if a parameterization of the cross section dependence from one grid point to another exists. In this section, we describe the details of a cross section scaling procedure that can be used to reinterpret results for a fixed coupling for s-channel mediator models. The studies in this section employ the POWHEG [**?**] generator.

The propagator for the s-channel exchange is written in a Breit-Wigner form as $\frac{1}{q^2 - M_{\rm med}^2 + iM_{\rm med}\Gamma}$, where q is the momentum transfer calculated from the two partons entering the hard process after the initial state radiation, which is equivalent to the momentum of the DM pair [9]. The size of the momentum transfer with respect to the mediator mass allows us to identify three cases:

- off-shell mediator, when $q^2 \gg M_{\rm med}^2$ leading to suppressed cross sections,
- on-shell mediator, when $q^2 \sim M_{\rm med}^2$ leading to enhanced cross sections,
- effective field theory (EFT) limit when $q^2 \ll M_{\rm med}^2$.

In the case of the off-shell mediator and the EFT limit, the first and second term in the propagator dominate, respectively, which reduces the dependence on the mediator width. Therefore, in these cases one can approximate the cross section as

$$\sigma \propto g_{\rm q}^2 g_\chi^2. \tag{17}$$

The on-shell regime is the most interesting one as it gives the best chances for a discovery at the LHC given the cross section enhancement. The propagator term with the width cannot be neglected in this case and, in the narrow width approximation which requires $\Gamma \ll M_{\rm med}$ (this is not necessarily the case in the benchmarks considered in the scans), one can integrate

$$\int \frac{ds}{(s - M_{\rm med}^2)^2 + M_{\rm med}^2\Gamma^2} = \frac{\pi}{M_{\rm med}\Gamma} \tag{18}$$

which further implies the cross section scaling

$$\sigma \propto \frac{g_{\rm q}^2 g_\chi^2}{\Gamma}. \tag{19}$$

The narrow width approximation is important here as it ensures an integration over parton distribution functions (PDFs) can be neglected. In other words,

[9] Using a running width and replacing the denominator of the propagator with $q^2 - M_{\rm med}^2 + iQ^2\frac{\Gamma}{M_{\rm med}}$ should be considered in the case of wide mediators [**?**].

it is assumed the integrand in Eq. 18 is non-zero only for a small region of s, such that the PDFs can be taken to be constant in this range. By simplifying the dependence of the minimal width on the couplings as $\Gamma \sim g_{\mathrm{q}}^2 + g_{\chi}^2$, one can approximate this scaling rule in the extreme cases as follows

$$\sigma \propto \frac{g_{\mathrm{q}}^2 g_{\chi}^2}{g_{\mathrm{q}}^2 + g_{\chi}^2} \xrightarrow{g_{\mathrm{q}} \ll g_{\chi}} g_{\mathrm{q}}^2 \tag{20}$$

$$\sigma \propto \frac{g_{\mathrm{q}}^2 g_{\chi}^2}{g_{\mathrm{q}}^2 + g_{\chi}^2} \xrightarrow{g_{\mathrm{q}} \gg g_{\chi}} g_{\chi}^2 \, . \tag{21}$$

However, it is important to keep in mind that this formula omits color and multiplicity factors as well as possible Yukawa suppression, and there is no simple scaling rule for how the cross section changes with the DM mass and the mediator mass, or for mediators with a large width, because PDFs matter in such cases as well. Therefore, the scaling procedure outlined above is expected to work only for fixed masses and fixed mediator width, assuming the narrow width approximation applies.

Figure 34 shows the minimal width over the mediator mass in the g_{q}–g_{χ} plane for vector and scalar mediators for $M_{\mathrm{med}} = 100$ GeV and 1000 GeV, taking $m_{\chi} = 10$ GeV. The individual colors indicate the lines of constant width, along which the cross section scaling may work for narrow mediators. The limiting case $\Gamma_{\mathrm{min}} = M_{\mathrm{med}}$ defines the upper values of the couplings below which the narrow width approximation can be considered and provides more stringent constraint than the perturbative limit $g_{\mathrm{q}} = g_{\chi} = 4\pi$. For vector and axial-vector mediators, the minimal width is predominantly defined by g_{q} due to the number of quark flavors and the color factor. On the contrary, both the SM and DM partial width have comparable contributions in case of scalar and pseudo-scalar mediators if the top quark channel is open ($M_{\mathrm{med}} > 2m_t$). However, mostly g_{χ} defines the minimal width for $M_{\mathrm{med}} < 2m_t$ due to the Yukawa-suppressed light quark couplings.

The performance of the cross section scaling is demonstrated in Fig. 35 where two mass points $M_{\mathrm{med}} = 100$ GeV and 1 TeV with $m_{\chi} = 10$ GeV are chosen

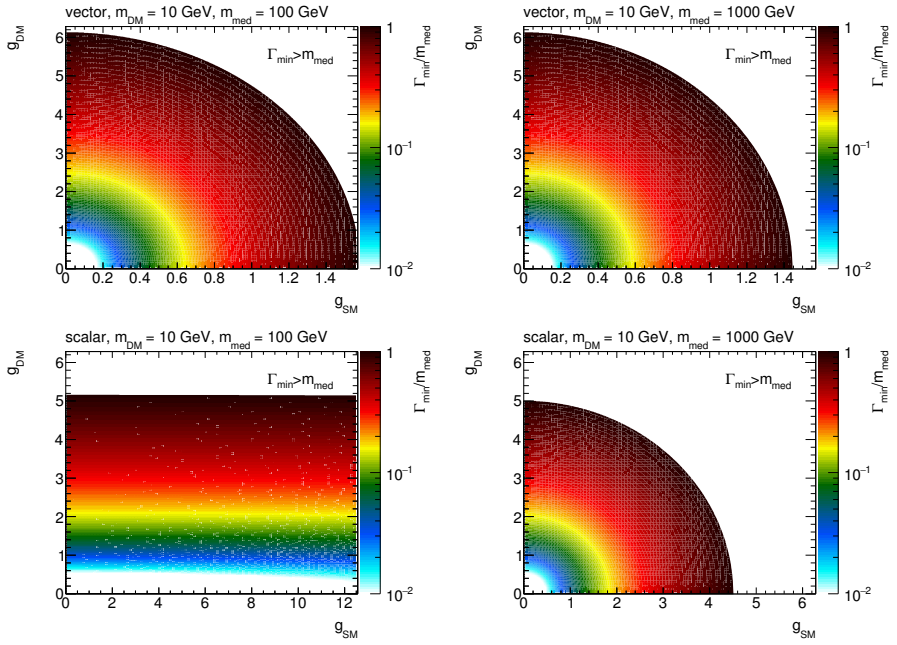

Figure 34: Minimal width over the mediator mass for vector (top) and scalar (bottom) mediators as a function of the individual couplings g_{q} and g_{χ}, assuming $M_{\mathrm{med}} = 100$ GeV (left) and $M_{\mathrm{med}} = 1$ TeV (right). $m_{\chi} = 10$ GeV is considered in all cases. Only the cases with $\Gamma_{\mathrm{min}} < M_{\mathrm{med}}$ are shown.

and rescaled from the starting point $g_q = g_\chi = 1$ according to Eq. 19 to populate the whole g_q–g_χ plane. This means the width is not kept constant in this test and this is done in purpose in order to point out deviations from the scaling when the width is altered. For each mass point, the rescaled cross section is compared to the generator cross section and the ratio of the two is plotted. For the given choice of the mass points, the scaling seems to work approximately within the precision of $\sim 20\%$ in the region where $\Gamma_{min} < M_{med}$. Constant colors indicate the lines along which the cross section scaling works precisely and there is a remarkable resemblance of the patterns shown in the plots of the mediator width. To prove the scaling along the lines of constant width works, one such line is chosen in Fig. 36 for a scalar mediator, defined by $M_{med} = 300$ GeV, $m_\chi = 100$ GeV, $g_q = g_\chi = 1$, and the rescaled and generated cross sections are found to agree within 3%.

4.1. Proposed parameter grid for cross-section scaling

We propose to deliver collider results in the g_q–g_χ plane using the following prescription, to ease reinterpretation through cross-section scaling:

- Since the shapes of kinematic quantities do not change for different couplings, use the acceptance and efficiency for the available $m_\chi = 50$ GeV, $M_{med} = 300$ GeV grid point from the M_{med}–m_χ plane for the scalar and pseudo-scalar mediator. In case of the vector and axial-vector mediator, use the grid point $m_\chi = 150$ GeV, $M_{med} = 1$ TeV.

- Generate additional samples in order to get generator cross sections only. For scalar and pseudo-scalar mediator, choose $m_\chi = 50$ GeV, $M_{med} = 300$ GeV with the following values for $g_q = g_\chi$: 0.1, 1, 2, 3. For vector and axial vector mediator, choose $m_\chi = 150$ GeV, $M_{med} = 1$ TeV with the following values for $g_q = g_\chi$: 0.1, 0.25, 0.5, 0.75, 1, 1.25, 1.5. The upper values are defined by the minimal width reaching the mediator mass.

- Rescale the generator cross sections for on-shell resonance production along the lines of constant width in order to populate the whole g_q–g_χ

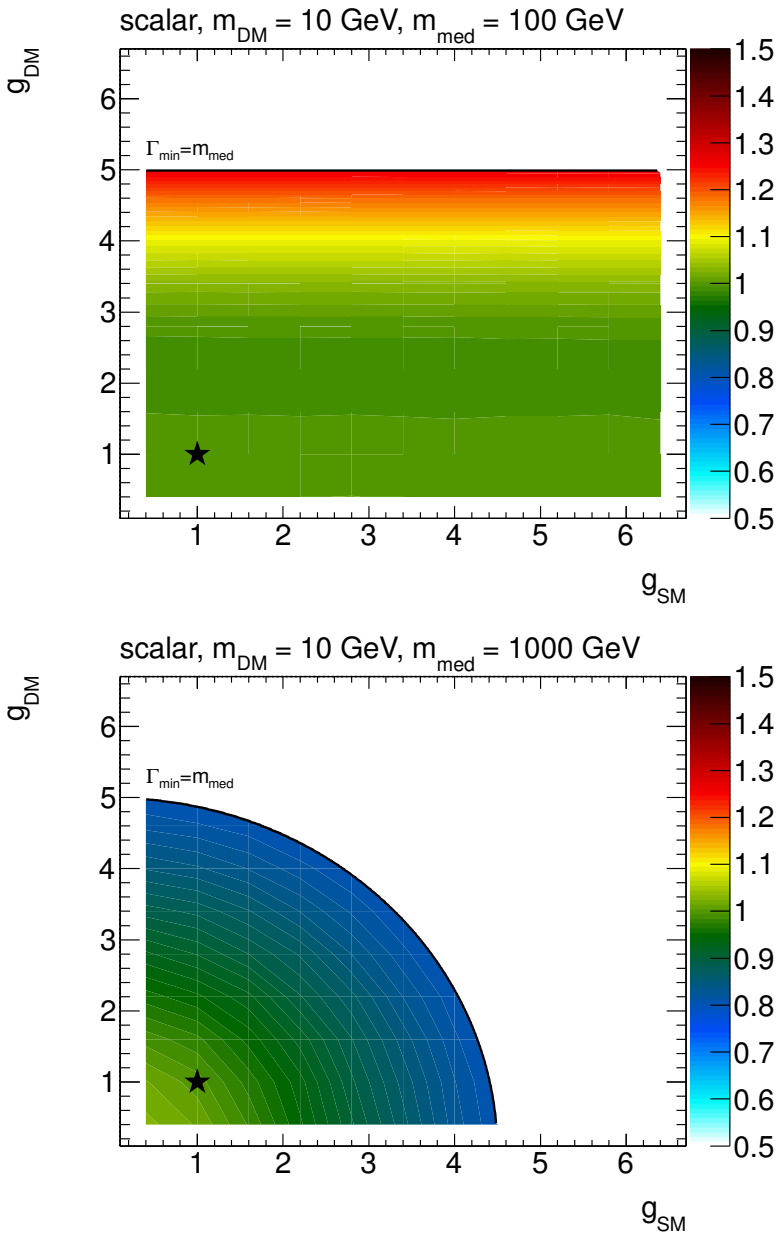

Figure 35: Ratio of the rescaled and generated cross sections in the g_{q}–g_{χ} plane. The point at $g_{\mathrm{q}} = g_{\chi} = 1$, taken as a reference for the rescaling, is denoted by a star symbol. Scalar model with $M_{\mathrm{med}} = 100$ GeV (left) and 1 TeV (right) is plotted for $m_{\chi} = 10$ GeV. The limiting case $\Gamma_{\mathrm{min}} = M_{\mathrm{med}}$ is indicated by a black line and no results are shown beyond.

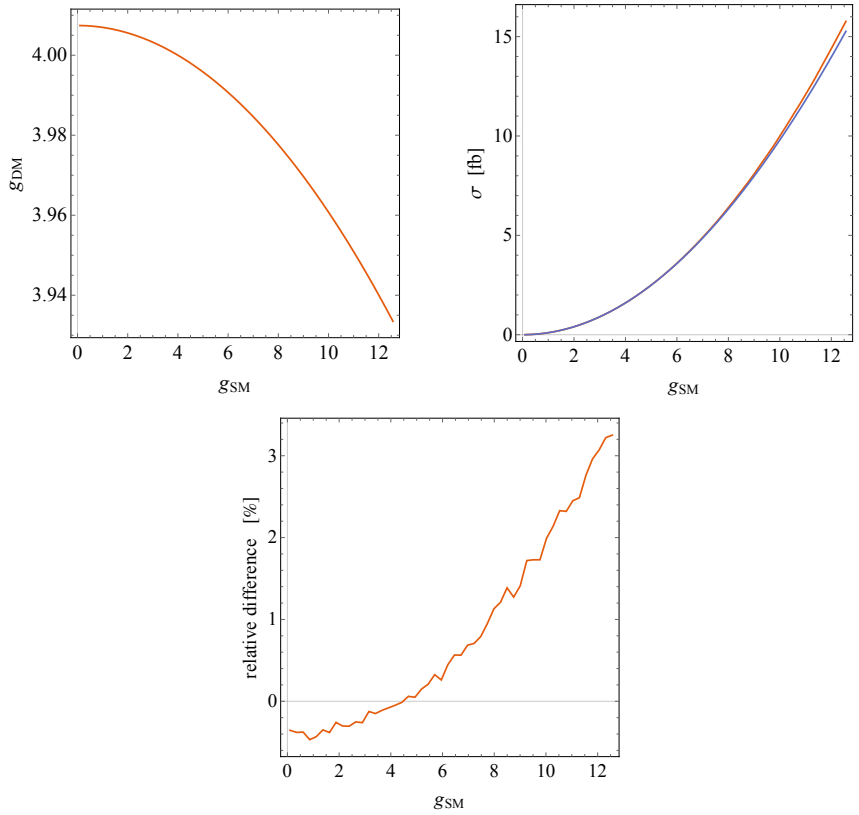

Figure 36: Scaling along the lines of constant width. The line of constant width for $M_{\mathrm{med}} = 300$ GeV and $m_\chi = 100$ GeV, intercepting $g_{\mathrm{q}} = g_\chi = 4$ is shown on left. The generated and rescaled cross sections are compared in the middle, the corresponding ratio is shown on right.

plane in the region $\Gamma_{\rm min} < M_{\rm med}$. The scaling follows from Eq. 19 which for the constant width implies:

$$\sigma' = \sigma \times \frac{g'^2_{\rm q} g'^2_{\chi}}{g^2_{\rm q} g^2_{\chi}} \ . \tag{22}$$

4.2. Rescaling to different mediator width

In general it is also important to consider a larger mediator width than $\Gamma_{\rm min}$ in order to accommodate additional interactions of the mediator with the visible and hidden sector particles [**? ?**]. If the narrow width approximation applies, the cross section scaling method described above can be used to reinterpret the results presented for the minimal width, since multiplying the width by factor n is equivalent to changing the coupling strength by factor $\sqrt{n}$, i.e.

$$\sigma(g_{\rm q}, g_{\chi}, n\Gamma_{\rm min}(g_{\rm q}, g_{\chi})) \propto \frac{g^2_{\rm q} g^2_{\chi}}{\Gamma_{\rm min}(\sqrt{n}g_{\rm q}, \sqrt{n}g_{\chi})} \ . \tag{23}$$

The cross section for the sample with couplings $g_{\rm q}$ and g_{χ} and modified mediator width $\Gamma = n\Gamma_{\rm min}$ can therefore be rescaled from a sample generated with the minimal width corresponding to the couplings scaled by $\sqrt{n}$ as described in the following formula.

$$\sigma(g_{\rm q}, g_{\chi}, n\Gamma_{\rm min}(g_{\rm q}, g_{\chi})) = \frac{1}{n^2}\sigma(\sqrt{n}g_{\rm q}, \sqrt{n}g_{\chi}, \Gamma_{\rm min}(\sqrt{n}g_{\rm q}, \sqrt{n}g_{\chi})) \tag{24}$$

The advantage of doing this is in the fact that no event selection and detector response needs to be simulated since the changes in couplings do not have an effect on the shapes of kinematic distributions.

It should be noted again that this procedure is only useful when the narrow width approximation applies. Care must be taken to ensure that is the case. For example, in the vector and axial-vector cases, one quickly breaks this approximation even for small n.

4.3. Additional considerations for $t\bar{t}$ and $b\bar{b}$+$\not{E}_T$ signatures

The cross-section scaling considerations shown in Sec. 4 still apply for the reactions in the scalar and psuedoscalar models with explicit b and t quarks. Here we detail the specific studies done for the $t\bar{t}$ model.